than that of wild-type mice, suggesting that *Angptl2*$^{-/-}$ mice were more likely to use lipids than carbohydrates for oxidation to create energy. There was also a trend of increased expression of lipid oxidation genes in the skeletal muscle of *Angptl2*$^{-/-}$ mice and increased UCP1 expression in brown adipose tissue (Figures S11D and S11F), which may account for the lower respiratory quotient, decreased triglyceride content of skeletal muscle, and decrease of whole-body fat in *Angptl2*$^{-/-}$ mice. On the other hand, the hepatic expression of lipogenic genes (SREBP-1c, FAS, and SCD1) was significantly decreased in *Angptl2*$^{-/-}$ mice (Figure S11G), which explains the decreased triglyceride content in the liver of these mice, although further studies will be needed to clarify the molecular mechanisms involved.

In summary, this study provided evidence that Angptl2 plays a key role in inflammation of adipose tissue via inflammatory vascular remodeling and recruitment of macrophages into adipose tissue. These findings suggest that Angptl2 may be an important part of the mechanism underlying adipose tissue inflammation that is involved in the pathogenesis of systemic insulin resistance related to obesity. The present findings should also lead to new treatment strategies for obesity and related insulin resistance.

EXPERIMENTAL PROCEDURES

Materials and additional methods are available in the Supplemental Experimental Procedures.

Animal Study

All experimental protocols were approved by the Ethics Review Committee for Animal Experimentation of Kumamoto University. Only male mice were used for the experiments. For the metabolic analyses, mice at 8 weeks of age were fed either a normal diet (CE-2; CLEA, Japan) or a high-fat diet (HFD-32; CLEA) for a period of 8 weeks. During the analyses, mice continued to feed on the same diet.

Human Studies

White adipose tissue samples were obtained from the intact adipose tissue surrounding the tumor resected from a patient with pancreatic carcinoma. Samples were fixed in 4% paraformaldehyde for 24 hr and embedded in paraffin. Sections 5 μm thick were cut and stained with an anti-Angptl2 polyclonal antibody (#383). Nuclei were counterstained with hematoxylin. A total of 98 volunteers working at Kumamoto University were enrolled in the study as the healthy group (persons with obesity [body mass index > 30] or diabetes were excluded). Blood samples were collected, and the plasma glucose, insulin, and CRP levels were measured. A total of 89 patients with type 2 diabetes were enrolled as the DM group. Their abdominal fat content was evaluated by magnetic resonance imaging. The HOMA-R index was calculated as the product of fasting plasma insulin (μU/ml) and fasting plasma glucose (mg/dl) divided by 405 (Matthews et al., 1985). The euglycemic-hyperinsulinemic clamp test was carried out according to a protocol described elsewhere (DeFronzo et al., 1979). A total of 109 patients with coronary artery disease (diagnosed by coronary angiography) were enrolled as the CAD group, and blood samples were collected. Twenty-seven obese diabetic men who had not previously received any antidiabetic agents, antihypertensive agents, or lipid-lowering drugs were treated with pioglitazone at a dose of 30 mg/day for 3 months. Before and after treatment, the abdominal fat content was evaluated by CT scanning, and fasting blood samples were collected to measure the levels of glucose, insulin, and CRP. Blood samples were also collected from 935 consecutive volunteers aged 27–84 years, who underwent medical checkups at the Japanese Red Cross Kumamoto Health Care Center. Serum or plasma levels of Angptl2 and Angptl4 were measured by ELISA. This study was approved by the Ethics Committees of Kumamoto University (healthy and CAD groups), Kobe University (DM group), Ryukyu University (pioglitazone study), and the Japanese Red Cross Kumamoto Health Care Center. Written informed consent was obtained from each subject.

SUPPLEMENTAL DATA

Supplemental Data include Supplemental Experimental Procedures, Supplemental References, 13 figures, one table, and four movies and can be found with this article online at http://www.cell.com/cell-metabolism/supplemental/S1550-4131(09)00232-0.

ACKNOWLEDGMENTS

We would like to thank Ms. K. Fukushima, I. Ishimatsu, R. Shindo, Y. Indo, S. Iwaki, and O. Takahashi for experimental assistance; and Drs. S. Fuchigami, K. Yasunaga, N. Yamaji, and A. Sakurai for experimental assistance and helpful discussion. This work was supported by Grants-in-Aid for Scientific Research on Priority Areas (17014078) from the Ministry of Education, Culture, Sports, Science and Technology of Japan; by Grants-in Aid for Scientific Research (B) (21390245) from Japan Society for Promotion of Science; by a grant from the Mochida Memorial Foundation; by a grant from the Takeda Science Foundation; by a grant from the Sumitomo Foundation; by a grant from the Uehara Memorial Foundation; and by a grant from the Cell Science Research Foundation.

Received: February 3, 2009
Revised: June 5, 2009
Accepted: August 10, 2009
Published: September 1, 2009

REFERENCES

Apovian, C.M., Bigornia, S., Mott, M., Meyers, M.R., Ulloor, J., Gagua, M., McDonnell, M., Hess, D., Joseph, L., and Gokce, N. (2008). Adipose macrophage infiltration is associated with insulin resistance and vascular endothelial dysfunction in obese subjects. Arterioscler. Thromb. Vasc. Biol. *28*, 1654–1659.

Bar-Sagi, D., and Hall, A. (2000). Ras and Rho GTPases: a family reunion. Cell *103*, 227–238.

Camenisch, G., Pisabarro, M.T., Sherman, D., Kowalski, J., Nagel, M., Hass, P., Xie, M.H., Gurney, A., Bodary, S., Liang, X.H., et al. (2002). ANGPTL3 stimulates endothelial cell adhesion and migration via integrin alpha v beta 3 and induces blood vessel formation in vivo. J. Biol. Chem. *277*, 17281–17290.

DeFronzo, R.A., Tobin, J.D., and Andres, R. (1979). Glucose clamp technique: a method for quantifying insulin secretion and resistance. Am. J. Physiol. *237*, E214–E223.

Dormond, O., Foletti, A., Paroz, C., and Ruegg, C. (2001). NSAIDs inhibit alpha V beta 3 integrin-mediated and Cdc42/Rac-dependent endothelial-cell spreading, migration and angiogenesis. Nat. Med. *7*, 1041–1047.

Dvorak, H.F., Senger, D.R., Dvorak, A.M., Harvey, V.S., and McDonagh, J. (1985). Regulation of extravascular coagulation by microvascular permeability. Science *227*, 1059–1061.

Eckel, R.H., Grundy, S.M., and Zimmet, P.Z. (2005). The metabolic syndrome. Lancet *365*, 1415–1428.

Friedl, P., and Weigelin, B. (2008). Interstitial leukocyte migration and immune function. Nat. Immunol. *9*, 960–969.

Fryer, B.H., and Field, J. (2005). Rho, Rac, Pak and angiogenesis: old roles and newly identified responsibilities in endothelial cells. Cancer Lett. *229*, 13–23.

Graves, K.L., and Roman, J. (1996). Fibronectin modulates expression of interleukin-1 beta and its receptor antagonist in human mononuclear cells. Am. J. Physiol. *271*, L61–L69.

Hato, T., Tabata, M., and Oike, Y. (2008). The role of angiopoietin-like proteins in angiogenesis and metabolism. Trends Cardiovasc. Med. *18*, 6–14.

Herrick, S., Blanc-Brude, O., Gray, A., and Laurent, G. (1999). Fibrinogen. Int. J. Biochem. Cell Biol. *31*, 741–746.

Hosogai, N., Fukuhara, A., Oshima, K., Miyata, Y., Tanaka, S., Segawa, K., Furukawa, S., Tochino, Y., Komuro, R., Matsuda, M., and Shimomura, I. (2007). Adipose tissue hypoxia in obesity and its impact on adipocytokine dysregulation. Diabetes *56*, 901–911.

Hynes, R.O. (2002). Integrins: bidirectional, allosteric signaling machines. Cell *110*, 673–687.

Ito, Y., Oike, Y., Yasunaga, K., Hamada, K., Miyata, K., Matsumoto, S., Sugano, S., Tanihara, H., Masuho, Y., and Suda, T. (2003). Inhibition of angiogenesis and vascular leakiness by angiopoietin-related protein 4. Cancer Res. *63*, 6651–6657.

Jackson, J.R., Seed, M.P., Kircher, C.H., Willoughby, D.A., and Winkler, J.D. (1997). The codependence of angiogenesis and chronic inflammation. FASEB J. *11*, 457–465.

Kadowaki, T., and Yamauchi, T. (2005). Adiponectin and adiponectin receptors. Endocr. Rev. *26*, 439–451.

Kanda, H., Tateya, S., Tamori, Y., Kotani, K., Hiasa, K., Kitazawa, R., Kitazawa, S., Miyachi, H., Maeda, S., Egashira, K., and Kasuga, M. (2006). MCP-1 contributes to macrophage infiltration into adipose tissue, insulin resistance, and hepatic steatosis in obesity. J. Clin. Invest. *116*, 1494–1505.

Kim, I., Moon, S.O., Koh, K.N., Kim, H., Uhm, C.S., Kwak, H.J., Kim, N.G., and Koh, G.Y. (1999). Molecular cloning, expression, and characterization of angiopoietin-related protein. angiopoietin-related protein induces endothelial cell sprouting. J. Biol. Chem. *274*, 26523–26528.

Klein, S., de Fougerolles, A.R., Blaikie, P., Khan, L., Pepe, A., Green, C.D., Koteliansky, V., and Giancotti, F.G. (2002). Alpha 5 beta 1 integrin activates an NF-kappa B-dependent program of gene expression important for angiogenesis and inflammation. Mol. Cell. Biol. *22*, 5912–5922.

Kubota, Y., Oike, Y., Satoh, S., Tabata, Y., Niikura, Y., Morisada, T., Akao, M., Urano, T., Ito, Y., Miyamoto, T., et al. (2005a). Cooperative interaction of Angiopoietin-like proteins 1 and 2 in zebrafish vascular development. Proc. Natl. Acad. Sci. USA *102*, 13502–13507.

Luster, A.D., Alon, R., and von Andrian, U.H. (2005). Immune cell migration in inflammation: present and future therapeutic targets. Nat. Immunol. *6*, 1182–1190.

Matthews, D.R., Hosker, J.P., Rudenski, A.S., Naylor, B.A., Treacher, D.F., and Turner, R.C. (1985). Homeostasis model assessment: insulin resistance and beta-cell function from fasting plasma glucose and insulin concentrations in man. Diabetologia *28*, 412–419.

McDonald, D.M. (1994). Endothelial gaps and permeability of venules in rat tracheas exposed to inflammatory stimuli. Am. J. Physiol. *266*, L61–L83.

Mettouchi, A., Klein, S., Guo, W., Lopez-Lago, M., Lemichez, E., Westwick, J.K., and Giancotti, F.G. (2001). Integrin-specific activation of Rac controls progression through the G(1) phase of the cell cycle. Mol. Cell *8*, 115–127.

Mokdad, A.H., Ford, E.S., Bowman, B.A., Dietz, W.H., Vinicor, F., Bales, V.S., and Marks, J.S. (2003). Prevalence of obesity, diabetes, and obesity-related health risk factors, 2001. JAMA *289*, 76–79.

Mosesson, M.W. (2005). Fibrinogen and fibrin structure and functions. J. Thromb. Haemost. *3*, 1894–1904.

Neels, J.G., and Olefsky, J.M. (2006). Inflamed fat: what starts the fire? J. Clin. Invest. *116*, 33–35.

Nishimura, S., Manabe, I., Nagasaki, M., Seo, K., Yamashita, H., Hosoya, Y., Ohsugi, M., Tobe, K., Kadowaki, T., Nagai, R., and Sugiura, S. (2008). In vivo imaging in mice reveals local cell dynamics and inflammation in obese adipose tissue. J. Clin. Invest. *118*, 710–721.

Oike, Y., Yasunaga, K., and Suda, T. (2004). Angiopoietin-related/angiopoietin-like proteins regulate angiogenesis. Int. J. Hematol. *80*, 21–28.

Oike, Y., Akao, M., Kubota, Y., and Suda, T. (2005a). Angiopoietin-like proteins: potential new targets for metabolic syndrome therapy. Trends Mol. Med. *11*, 473–479.

Oike, Y., Akao, M., Yasunaga, K., Yamauchi, T., Morisada, T., Ito, Y., Urano, T., Kimura, Y., Kubota, Y., Maekawa, H., et al. (2005b). Angiopoietin-related growth factor antagonizes obesity and insulin resistance. Nat. Med. *11*, 400–408.

Perona, R., Montaner, S., Saniger, L., Sanchez-Perez, I., Bravo, R., and Lacal, J.C. (1997). Activation of the nuclear factor-kappaB by Rho, CDC42, and Rac-1 proteins. Genes Dev. *11*, 463–475.

Roman, J., Ritzenthaler, J.D., Boles, B., Lois, M., and Roser-Page, S. (2004). Lipopolysaccharide induces expression of fibronectin alpha 5 beta 1-integrin receptors in human monocytic cells in a protein kinase C-dependent fashion. Am. J. Physiol. Lung Cell. Mol. Physiol. *287*, L239–L249.

Rose, D.M., Alon, R., and Ginsberg, M.H. (2007). Integrin modulation and signaling in leukocyte adhesion and migration. Immunol. Rev. *218*, 126–134.

Schenk, S., Saberi, M., and Olefsky, J.M. (2008). Insulin sensitivity: modulation by nutrients and inflammation. J. Clin. Invest. *118*, 2992–3002.

Sulciner, D.J., Irani, K., Yu, Z.X., Ferrans, V.J., Goldschmidt-Clermont, P., and Finkel, T. (1996). rac1 regulates a cytokine-stimulated, redox-dependent pathway necessary for NF-kappaB activation. Mol. Cell. Biol. *16*, 7115–7121.

Weisberg, S.P., Hunter, D., Huber, R., Lemieux, J., Slaymaker, S., Vaddi, K., Charo, I., Leibel, R.L., and Ferrante, A.W., Jr. (2006). CCR2 modulates inflammatory and metabolic effects of high-fat feeding. J. Clin. Invest. *116*, 115–124.

Ye, J. (2009). Emerging role of adipose tissue hypoxia in obesity and insulin resistance. Int. J. Obes. *33*, 54–66.

Molecular Biology of the Cell
Vol. 20, 3115–3124, July 1, 2009

Zyxin Mediates Actin Fiber Reorganization in Epithelial–Mesenchymal Transition and Contributes to Endocardial Morphogenesis

Masaki Mori,* Hironori Nakagami,* Nobutaka Koibuchi,† Koichi Miura,‡ Yoichi Takami,* Hiroshi Koriyama,* Hiroki Hayashi,* Hisataka Sabe,§ Naoki Mochizuki,‡ Ryuichi Morishita,‖ and Yasufumi Kaneda*

*Division of Gene Therapy Science and ‖Department of Clinical Gene Therapy, Graduate School of Medicine, Osaka University, Osaka 565-0871, Japan; †Department of Advanced Clinical Science and Therapeutics, University of Tokyo, Tokyo 113-8656, Japan; ‡Department of Structural Analysis, National Cardiovascular Center Research Institute, Osaka 565-8565, Japan; and §Department of Molecular Biology, Osaka Bioscience Institute, Osaka 565-0874, Japan

Submitted January 15, 2009; Revised April 27, 2009; Accepted May 4, 2009
Monitoring Editor: Asma Nusrat

Epithelial–mesenchymal transition (EMT) confers destabilization of cell–cell adhesion and cell motility required for morphogenesis or cancer metastasis. Here we report that zyxin, a focal adhesion-associated LIM protein, is essential for actin reorganization for cell migration in TGF-β1–induced EMT in normal murine mammary gland (NMuMG) cells. TGF-β1 induced the relocation of zyxin from focal adhesions to actin fibers. In addition, TGF-β1 up-regulated zyxin via a transcription factor, Twist1. Depletion of either zyxin or Twist1 abrogated the TGF-β1–dependent EMT, including enhanced cell motility and actin reorganization, indicating the TGF-β1-Twist1-zyxin signal for EMT. Both zyxin and Twist1 were predominantly expressed in the cardiac atrioventricular canal (AVC) that undergoes EMT during heart development. We further performed ex vivo AVC explant assay and revealed that zyxin was required for the reorganization of actin fibers and migration of the endocardial cells. Thus, zyxin reorganizes actin fibers and enhances cell motility in response to TGF-β1, thereby regulating EMT.

INTRODUCTION

Epithelial–mesenchymal transition (EMT) is an essential event during embryogenesis for the formation of many tissues including the mesoderm, for migration of neural crest cells, and for development of the heart valves and septa. The picture emerging from diverse EMT-related studies suggests that precise molecular and cellular control of EMT is complex and context-dependent (Nakaya *et al.*, 2008). An example of developmentally regulated EMT occurs during the initial stages of cardiac morphogenesis. At embryonic day 9.5 (E9.5), endocardial cells undergo EMT ("endocardial EMT"); delaminating from the endothelial sheet, invading the matrix tissue called cardiac jelly, and engaging in endocardial cushion cellularization required for valve and septum formation (Chang *et al.*, 2004). Because a number of congenital heart diseases are caused by abnormal atrioventricular canal (AVC) development (Bruneau, 2008), understanding of the molecular basis of AVC morphogenesis has been long sought, but still not fully achieved. Several EMT-inducing transcription factors such as Snail (Cano *et al.*, 2000) and Twist1 (Ma *et al.*, 2005) are expressed in endocardium during development. Although among them, Twist1 is well analyzed as a potent EMT inducer during cancer metastasis (Yang *et al.*, 2004); however, the role for Twist1 in AVC development is not fully understood.

An important hallmark of EMT is an increase in cell motility with actin cytoskeletal rearrangement. On EMT induction, the structure of actin cytoskeleton changes dynamically from cortical actin network to stress fiber (Zavadil and Bottinger, 2005). Cell motility also depends on the adhesion of the cell to the substratum where the integrin family molecules bind to the extracellular matrix to form focal adhesion complexes. Stress fibers link the focal adhesion to retract the cells. Furthermore, the nascent focal complexes at the leading edge of the migrating cells are needed for cell crawling by connecting the actin fibers between the front and rear focal adhesions. Thus, coordinated control of the various focal adhesion proteins is important for actin fiber reorganization. Among focal adhesion molecules, paxillin, focal adhesion kinase (FAK) and Hic-5 are reported to be involved in EMT (Hetey *et al.*, 2005; Tumbarello *et al.*, 2005). EMT induction in normal murine mammary gland (NMuMG) cells by TGF-β1 induces the phosphorylation and recruitment of paxillin to focal adhesions and the expression of Hic-5 (Tumbarello *et al.*, 2005).

Transforming growth factor β (TGF-β) is a potent EMT inducer and is implicated in a broad kind of EMT in cancer

This article was published online ahead of print in *MBC in Press* (http://www.molbiolcell.org/cgi/doi/10.1091/mbc.E09–01–0046) on May 13, 2009.

Address correspondence to: Hironori Nakagami (nakagami@gts.med.osaka-u.ac.jp) or Yasufumi Kaneda (kaneday@gts.med.osaka-u.ac.jp).

Abbreviations used: AVC, atrioventricular canal; EMT, epithelial–mesenchymal transition; NMuMG, normal murine mammary gland.

metastasis, tissue fibrosis, or tissue morphogenesis (Zavadil and Bottinger, 2005). TGF-β was first described as an inducer of EMT in normal mammary epithelial cells (Miettinen *et al.*, 1994), and murine mammary epithelial cells treated with TGF-β undergo a complete EMT (Thiery, 2003). Accumulating evidences revealed the involvement of TGF-β in vital steps during development (Sanford *et al.*, 1997; Bartram *et al.*, 2001; Sridurongrit *et al.*, 2008).

Zyxin belongs to a LIM protein family and harbors distinct actin polymerization activity independent of the Arp2/3 complex (Fradelizi *et al.*, 2001). Zyxin has three tandem LIM domains in its C terminus that support specific protein interactions (Schmeichel and Beckerle, 1994) and targeting to focal adhesions (Nix *et al.*, 2001). The proline-rich N-terminal domain called ActA mediates actin polymerization (Fradelizi *et al.*, 2001). Zyxin locates primarily at focal adhesions and regulates actin cytoskeleton dynamics, cell movement, and signal transduction (Beckerle, 1998; Kadrmas and Beckerle, 2004). Despite the understanding of zyxin, its role in the cellular actin rearrangement and its function in vivo is still unknown. A role for zyxin during development also remains to be elucidated.

In this study, we investigated the function of zyxin in TGF-β1–induced EMT and the EMT during heart morphogenesis and explored the requirement of zyxin in TGF-β1–dependent EMT and the contribution of zyxin to EMT for valvulogenesis in the heart.

Here, we show that zyxin regulates EMT by accelerating cell motility through controlling actin fiber reorganization in cultured epithelial cells and the endocardial cells of the embryonic heart.

MATERIALS AND METHODS

Cell Culture

NMuMG cells were obtained from ATCC (Manassas, VA) and maintained in DMEM supplemented with 10% FCS and 10 μg/ml insulin. We cloned the cells by limiting dilution and obtained 13 different clones. Among them, we used a cell line designated C7 that showed typical epithelial morphology and robust response to TGF-β1. The cells were maintained in DMEM (Nacalai Tesque, Tokyo, Japan) supplemented with 10% fetal bovine serum (FBS). TGF-β1–stimulation experiments were performed with recombinant human TGF-β1 (2 ng/ml; R&D Systems, Minneapolis, MN).

Deletion Mutants and Retroviral Vector Construction

Zyxin deletion mutants were generated by PCR amplifying the amino acid 1-375 (ΔLIM) or aa 376-564 (LIM only) region and inserting into pCAGIP-EGFP (enhanced green fluorescent protein) vector.

pCX4 puro vector was kindly provided by Tsuyoshi Akagi (Akagi *et al.*, 2003). pCX4 puro-EGFP-Snail, pCX4 puro-EGFP-Twist1, or pCX4 puro-HMGA2 were generated by inserting the full-length Snail cDNA from pCAGGS-EGFP-Snail, Twist1 cDNA from pCAGIP-Twist1 (Hayashi *et al.*, 2007), or HMGA2 cDNA from pENTR-HMGA2 into the pCX4 puro vector, respectively. Each plasmid above was cotransfected with pGP and pE-eco (Takara Bio, Tokyo, Japan) into BOSC to produce ecotropic retrovirus vector.

Immunocytochemistry

NMuMG-C7 cells were plated onto collagen-coated glass-bottom dishes (MatTek, Ashland, MA). The cells were fixed in 4% paraformaldehyde (PFA), permeabilized in 0.1% Triton X-100 for 5 min, and probed with mouse anti-zyxin antibody (1:40, 164D4, Synaptic Systems; 1:100, clone ZOL301, Sigma-Aldrich, St. Louis, MO), mouse anti-E-cadherin antibody (1:50, clone 36, BD Biosciences, San Jose, CA), mouse anti-N-cadherin antibody (1:50, clone 32, BD Biosciences), and rabbit anti-ZO-1-antibody (1:100, 61-7300, Invitrogen, Carlsbad, CA). The primary antibody was detected by goat anti-mouse-Alexa 488, goat anti-mouse-Alexa 546, or goat anti-rabbit-Alexa 546 (1:1000, Invitrogen). Nuclei were stained with 4′-6-diamidino-2-phenylindole (DAPI, Invitrogen). F-actin was stained with Alexa Fluor 546-phalloidin (Invitrogen).

Fluorescence Imaging

NMuMG-C7 cells were stably transfected with pCAGIP-EGFP-zyxin plasmid. Fluorescence images were recorded with a Nikon eclipse TE300 inverted microscope (Melville, NY) or with a confocal microscope with a Bio-Rad laser scanning system (Radiance 2100; Richmond, CA) coupled to a Nikon eclipse TE2000-U inverted microscope with a 60× oil immersion objective lens. For time-lapse recording of zyxin images, the cells were grown in 35-mm glass-bottom dishes (MatTek) and placed in a CO_2 chamber (Model CZI-3; Zeiss) at 37°C, attached to the stage of an inverted microscope (Axiovert 200; Zeiss). Images were acquired every 3 min using a 40 × 1.3 NA objective lens (Plan-NEOFLUAR, Zeiss) and a CCD camera (model HRm; Zeiss), and analyzed using Axiovision software (version 4.6, Zeiss).

SDS-PAGE and Western Blot Analysis

Cells were harvested in a RIPA lysis buffer. Protein concentration was determined by the method of Lowry (Lowry *et al.*, 1951). Protein samples (10 μg per lane) were separated by SDS-PAGE and transferred to a Hybond-P PVDF membrane (GE Healthcare, Little Chalfont, Buckinghamshire, England). Western blot was performed with the following antibodies: anti-zyxin (1:1000, ZOL301, Sigma-Aldrich), anti-vinculin (1:1000, V9264), anti-β-actin (1:5000, AC-15), anti-E-cadherin (1:5000, clone 36, BD Biosciences), anti-N-cadherin (1:5000, clone 32), anti-paxillin (1:1000, clone 165), anti-FAK (1:200, clone 77), anti-p130Cas (1:1000, clone 21), anti-Hic-5 (1:200, clone 34), anti-GFP (1:1000, 598, MBL, Nagoya, Japan), anti-HMGA2 (1:200, ab41878, Abcam, Cambridge, MA) and anti-GAPDH (1:5000, 6C5). All secondary antibodies were horseradish peroxidase conjugated (GE Healthcare) and were used at 1:1000 dilution. Immunoreactive bands were detected with Chemi-LumiOne L (Nacalai Tesque). Quantification was done by densitometry using ImageJ software (NIH; http://rsb.info.nih.gov/ij/).

Modified Boyden's Chamber Assay

Modified Boyden's chamber assay was carried out as previously described (Saito *et al.*, 2006). Briefly, 27 μl DMEM with 10% FBS was added to the lower chamber, and 50 μl of cell suspension (5×10^5 cells/ml) in DMEM with 10% FBS was added to the upper chamber. After 4 h of incubation, the cells on the lower side of the membrane were stained with Diff-Quick (Sysmex, Hyogo, Japan) to facilitate visualization and counting of cells. The count was done in eight randomly chosen fields.

RNA Interference Experiments

Zyxin or Twist1 Stealth small interfering RNA (siRNA) oligonucleotides were purchased from Invitrogen. The double-strand RNA (dsRNA) oligonucleotides against zyxin were as follows: (sense) 5′-AACAAAUGGAGUGGCAACUGGUGGG-3′ and (antisense) 5′-CCCACCAGUUGCCACUCCAUUUGUU-3′. The dsRNA oligonucleotides against Twist1 were as follows: (sense) 5′-UUGAGGGUCUGAAUCUUGCUCAGCU-3′ and (antisense) 5′-AGCUGAGCAAGAUUCAGACCCUCAA-3′. The scrambled siRNA oligonucleotides were as follows: (sense) 5′-UUCCUCAAUAGAUGCGUGUTT-3′ and (antisense) 5′-ACACGCAUCUAUUGAGGAATT-3′. These sequences did not correspond to any sequence in the mouse genome when subjected to a BLAST search. Transfections were carried out using Lipofectamine 2000 (Invitrogen), according to the manufacturer's instructions.

RT-PCR Analysis and Real-Time PCR Quantification

Total RNA was isolated using an RNeasy RNA isolation kit (QIAGEN, Valencia, CA). cDNA was synthesized using High Capacity cDNA Reverse Transcription Kit (Applied Biosystems, Foster City, CA). The sequences of PCR primers are shown in the Supplementary Table SI. The reactions were performed as follows: 98°C for 30 s; 25 cycles of 98°C for 10 s, 52°C for 30 s, and 72°C for 60 s. PCR products were separated in a 1.5% agarose gel. Real-time PCR was performed using an Applied Biosystems 7900 HT Fast Real-Time PCR system with TaqMan Probe for zyxin (Mm00496120_m1) and GAPDH (Mm99999915_g1) and TaqMan Universal PCR Master Mix (Applied Biosystems). The reactions were incubated at 95°C for 10 min followed by 40 cycles of 95°C for 15 s and 60°C for 1 min. The relative expression level was calculated from a standard curve obtained by using log dilutions of cDNA containing the gene of interest. The average of two independent analyses for each gene and sample was calculated and was normalized to the endogenous reference control gene GAPDH.

In Situ Hybridization

In situ hybridization was performed as previously described (Koibuchi and Chin, 2007). The cDNAs used for generation of Dig-labeled mouse riboprobes were *zyxin* (nucleotides 2002-2404; GenBank no. NM_011777) and *Twist1* (nucleotides 644-1524; GenBank no. NM_011658).

Lentivirus Vector

pcDNA6.2-shZyxin and pcDNA6.2-shLacZ were generated by inserting the oligonucleotide containing the specific siRNA target sequence into pcDNA6.2 vector (Invitrogen). pLenti6-shZyxin and pLenti6-shLacZ were generated from pcDNA6.2 constructs. Lentivirus was generated by cotransfection of the above construct with packaging plasmids into 293FT cells according to the

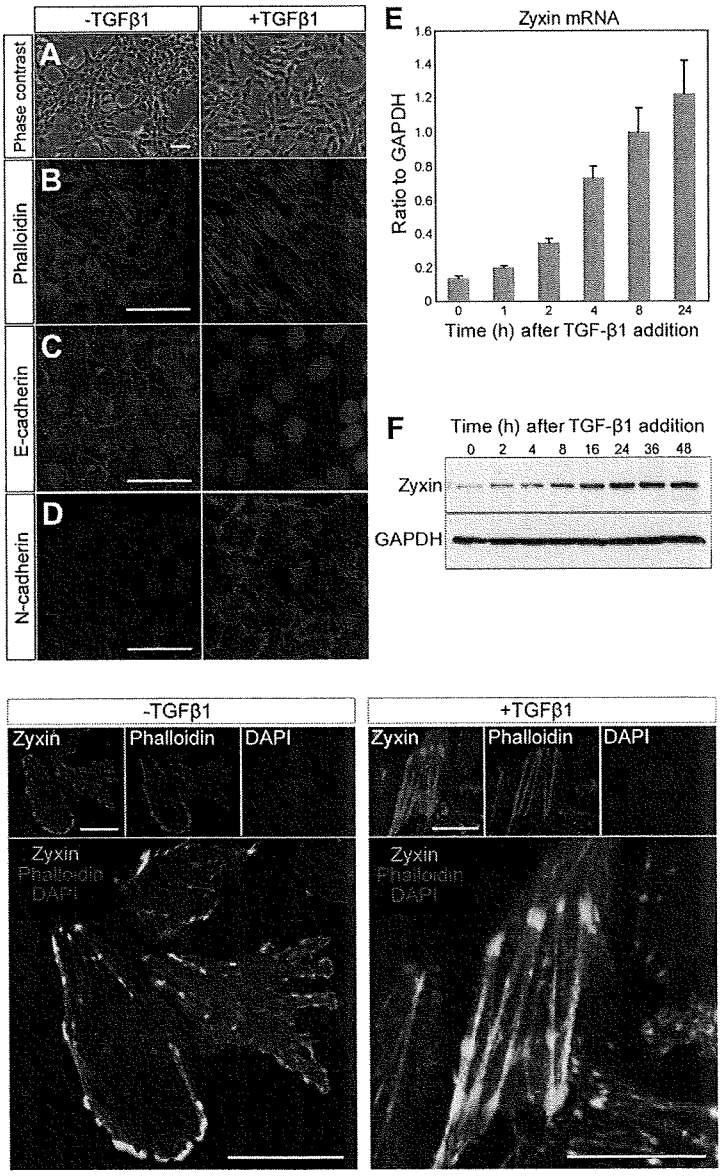

Figure 1. Zyxin is up-regulated and relocates to actin stress fibers in TGF-β1–induced EMT. (A–D) TGF-β1–induced in vitro EMT in NMuMG-C7 cells. NMuMG-C7 cells treated with TGF-β1 for 24 h exhibit the cell scattering (A), actin stress fiber formation (B), down-regulation of E-cadherin (C), and up-regulation of N-cadherin (D). Scale bars, 100 μm. (E) Real-time PCR analysis of zyxin mRNA in NMuMG-C7 cells treated with TGF-β1. Results are shown as the mean ± SEM (n = 3). (F) Immunoblot analysis of zyxin in NMuMG-C7 cells treated with TGF-β1. GAPDH was used as a loading control. (G) TGF-β1 induced zyxin relocation from focal adhesions to actin fibers. Confocal microscopy of EGFP-tagged zyxin (green) in NMuMG-C7 cells treated or not with TGF-β1 for 24 h. Zyxin locates at focal adhesions before TGF-β1 treatment and mobilizes to actin fibers after the treatment (Also see Supplementary Video 1). The cells were counterstained with phalloidin (red) and DAPI (blue). Scale bars, 50 μm.

manufacturer's instruction (Invitrogen). The sequences of shZyxin DNA oligo and shLacZ control oligo are available in the Supplementary Table SII.

Ex Vivo EMT Assay

The experiments were approved by the Ethics Committee for Animal Experiments of Osaka University Graduate School of Medicine. C57BL/6 mice were purchased from Charles River Breeding Laboratories. The ex vivo EMT assay was performed as described (Camenisch *et al.*, 2002) with some modifications. After putting E9.5 AVC explants on collagen gels, lentivirus-containing medium was added and incubated for 24 h. Then the explants were incubated with M199 media (Invitrogen/BRL, Rockville, MD) supplemented with 0.01% insulin, transferrin and selenium (ITS, Invitrogen/BRL) for 48 h, before determining the extent of outgrowth and matrix invasion. The criteria for "Migratory" were the appearance of the stellate cells migrating outward, frequently invading the collagen gel matrix. The criteria for "Nonmigratory" were the appearance of polygonal cells that form cobblestone-like colonies on the gel surface (Camenisch *et al.*, 2002). XZ confocal images were acquired to visualize collagen gel invasion. Cells that migrated into the collagen gel were stained with DAPI and counted in randomly collected areas. Phalloidin staining of the explants was done after the fixation with 4% PFA for 20 min on the collagen gel.

Statistics

Statistical analysis was performed with StatView 5.0 software (SAS Institute, Cary, NC). All results were expressed as mean ± SEM. Data were compared using ANOVA, followed by the Dunnett test for pairwise comparisons against control and by the Tukey test for multiple comparisons. Significance was defined as $p < 0.05$.

RESULTS

Zyxin Is Up-Regulated in TGF-β1–induced EMT and Mobilizes to Actin Fibers

Normal murine mammary gland (NMuMG) cells undergo EMT upon treatment with TGF-β1 (Tumbarello *et al.*, 2005). As reported, original NMuMG cells have heterogeneous morphology and responsiveness to TGF-β1. Thus, we cloned the cells by limiting dilution and established a cell line of NMuMG cells named NMuMG-C7, which altered the morphology in response to TGF-β1. On TGF-β1 treatment, NMuMG-C7 cells exhibited a series of EMT hallmarks such

as cell scattering (Figure 1A), actin stress fiber formation (Figure 1B), down-regulation of E-cadherin (Figure 1C), and up-regulation of N-cadherin (Figure 1D). We observed that TGF-β1 up-regulated zyxin mRNA (Figure 1E) and induced expression of zyxin (Figure 1F) in a time-dependent manner, suggesting the possible participation of zyxin in TGF-β1–dependent EMT. An increase of zyxin protein was seen as early as 2 h after treatment and was dramatically augmented later on.

To study how zyxin participates in TGF-β1–dependent EMT, we examined the localization of zyxin using EGFP-tagged zyxin before and after the TGF-β1 treatment. Previous reports confirmed the localization of EGFP-tagged zyxin corresponded to the endogenous zyxin (Nix *et al.*, 2001; Hotulainen and Lappalainen, 2006). Without stimulation, consistent with a previous report (Yoshigi *et al.*, 2005), zyxin localized to focal adhesions and focal complexes in the lamellipodia (Figure 1G, −TGF-β1). Of note, upon TGF-β1 stimulation, zyxin mobilized from focal adhesions to actin fibers (Figure 1G, +TGF-β1). The localization of zyxin in confluent cells was shown in Supplementary Figure S1. Time-lapse imaging revealed the translocation of zyxin to actin fibers in NMuMG-C7 cells treated with TGF-β1 (Supplementary Video 1). These findings lead us to assume the switch of the role for zyxin from the regulation of cell-extracellular matrix adhesion to that of actin fibers and suggest the involvement of zyxin in EMT.

Zyxin Is Required for Cell Migration and Actin Fiber Reorganization in EMT

To assess the requirement of zyxin in TGF-β1–induced EMT, we performed knockdown experiments of zyxin. The effectiveness of zyxin siRNA was confirmed in NMuMG-C7 cells (Figure 2A). TGF-β1 induced the expression of N-cadherin and reduced the expression of E-cadherin (Figure 2A). Depletion of zyxin affected the expression of neither E-cadherin nor N-cadherin and altered the localization of neither E-cadherin nor N-cadherin (Figure 2A and Supplementary Figure S2). We further assessed the effect of depletion of zyxin on TGF-β1–dependent cell motility. Knockdown of zyxin almost completely abolished TGF-β1–induced migration (Figure 2, B and C). These results indicate that zyxin is essential for TGF-β1–induced migration, a hallmark of EMT. Next, we examined the effect of zyxin depletion on actin cytoskeleton by phalloidin staining. Polarized epithelial cells including NMuMG cells have distinct actin networks in the apical and the basal side of the cells (Supplementary Figure S3). The apical actin fibers adherent to adherens junctions (Yonemura *et al.*, 1995; Vasioukhin *et al.*, 2000; Perez-Moreno *et al.*, 2003) and the basal actin stress fibers adherent to focal adhesions. We found that TGF-β1 induced both apical and basal actin fiber formation (Figure 2, E and I). Knockdown of zyxin resulted in inhibition of actin fiber formation at the basal level and, to a lesser extent, at the apical level. (Figure 2, G and K). To examine how essential zyxin was in EMT, we carried out rescue experiments using EGFP-tagged zyxin mutants (Figure 2L). The endogenous zyxin was depleted with short hairpin RNA (shRNA) that targets 3′ untranslated region (UTR) of zyxin mRNA (Figure 2M). The expression of exogenous zyxin mutants were confirmed (Figure 2M). The formation of actin stress fibers induced by TGF-β1 was rescued by the expression of EGFP-tagged full-length (FL) zyxin construct, supporting the specificity of zyxin siRNA and shRNA against zyxin. To the contrary, ΔLIM mutant dispersed in cytosol and failed to rescue. LIM only mutant exhibited localization to cytosol, focal adhesions, and nuclei and failed to rescue. Zyxin has ActA sequence in its N terminus, which has a distinct actin fiber polymerization activity (Fradelizi *et al.*, 2001), and in LIM domains, which is necessary for targeting to focal adhesions (Nix *et al.*, 2001). These experiments suggested that in the induction of EMT, both the localization and the activity were essential for zyxin. These findings suggest that zyxin is involved in TGF-β1–dependent EMT by regulating cell migration via controlling actin fiber formation. Considering that one of the most important features of EMT is the acquisition of motility (Thiery, 2003; Sung *et al.*, 2007), Zyxin appears to be essential for the progression of EMT.

Zyxin Is Expressed in AVC of Developing Heart and Valves in Mice

We sought the physiological role for zyxin in EMT. During development, EMT occurs during AVC morphogenesis that gives rise to valves and septa. We therefore investigated the expression of zyxin during development by in situ hybridization in mouse fetus. We found that zyxin was strongly expressed in AVC at E13.5 (Figure 3A, arrowhead). We examined the expression of zyxin in more detail during development and revealed that its expression at AVC was induced during development, peaked in AVC at E13.5 and waned in valves and septa at E14.5 (Figure 3B, arrowhead). These expression patterns of zyxin prompted us to assume that zyxin was involved in the endocardial EMT and that the cells expressing zyxin contributed to valvulogenesis. We further examined the expression of Twist1 and found the concordance of the expression between Twist1 and zyxin in AVC (Figure 3B). These findings are in agreement with the in vitro results of zyxin regulation by Twist1 (see below). Furthermore, analyses in adults revealed the expression of zyxin in valves (Figure 3C, arrowhead). These findings imply that zyxin-expressing cells that undergo endocardial EMT participate in valvulogenesis.

Next, we examined whether the involvement of zyxin in TGF-β1-EMT was similarly seen in vascular endothelial cells (Supplementary Figure S4) in vitro. TGF-β1 induced cell scattering and actin fiber formation in murine vascular endothelial cells (Supplementary Figure S4A). Knockdown of zyxin (Supplementary Figure S4B) repressed the actin fiber formation induced by TGF-β1 (Supplementary Figure S4C). Moreover, in bovine arterial endothelial cells, TGF-β1 treatment induced the cell shape change into fusiform (Supplementary Figure S4D) and up-regulation of zyxin (Supplementary Figure S4E).

Zyxin Is Required for Morphogenetic Movement of the Endocardial Cells

To understand how zyxin regulates EMT in the endocardial cells, we performed an ex vivo EMT assay (Figure 4A). The AVC explants isolated from E9.5 embryos recapitulate the process of EMT extracorporeally (Runyan and Markwald, 1983). We generated lentivirus vector expressing either zyxin shRNA or control LacZ shRNA to evaluate the effect of loss of zyxin expression in endocardial EMT. The efficacy of knockdown was confirmed after zyxin shRNA transduction (Figure 4B). The transduction efficiency was more than 85% by the estimation on the basis of EGFP fluorescence coexpressed on a single transcript (Figure 4C). The explants transduced with control shLacZ showed extensive radial migration of stellate cells with abundant protrusions (Figure 4D, LacZ shRNA). In contrast, the explants transduced with shZyxin showed significantly reduced cell migration and exhibited cobblestone-like appearance composed of polygonal cells (Figure 4D, zyxin shRNA). Although 76% of the explants transduced with shLacZ showed robust outgrowth

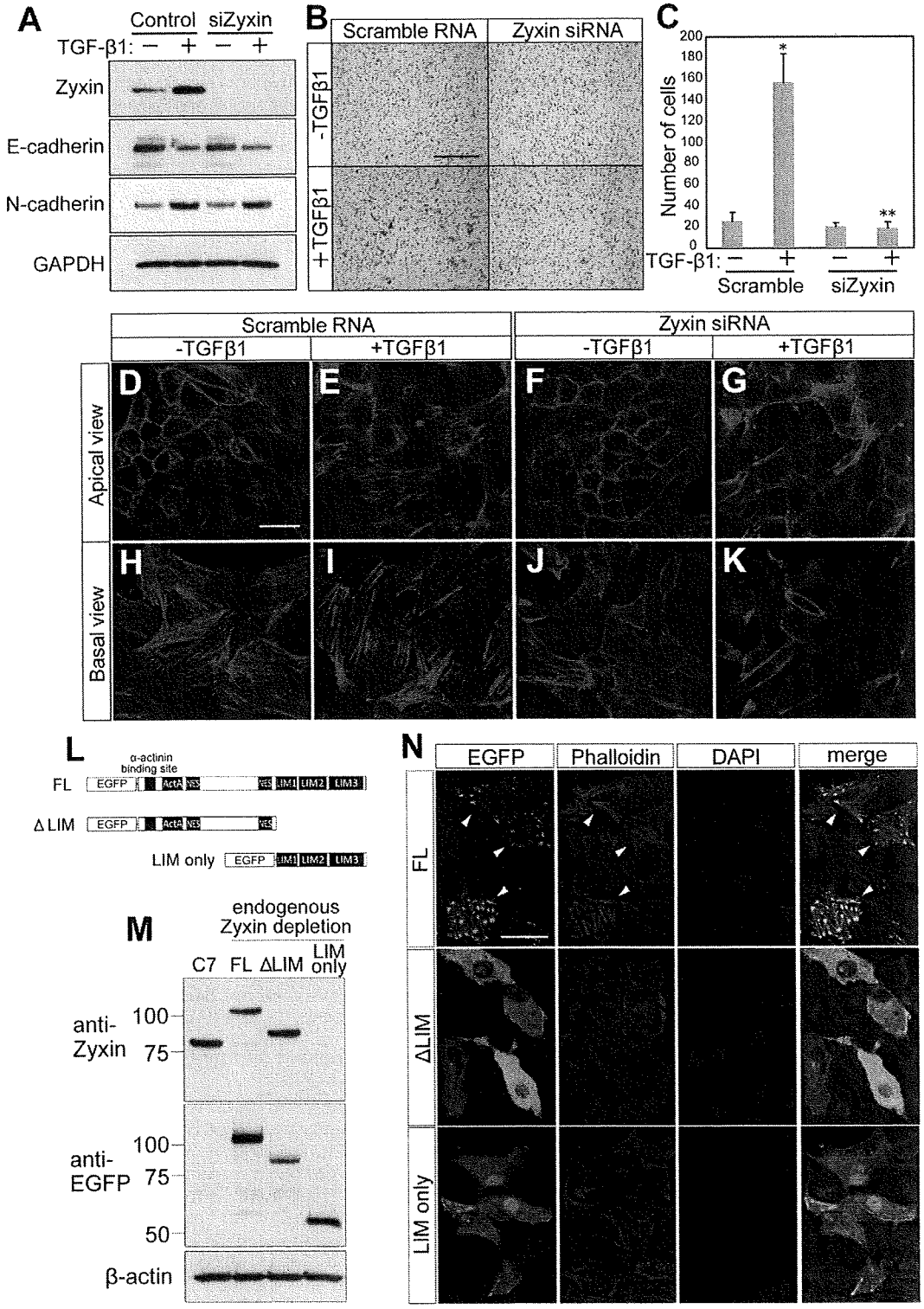

Figure 2. Zyxin is essential for cell migration and actin fiber reorganization in TGF-β1–induced EMT. (A) Immunoblot analysis of zyxin and E-and N-cadherin in NMuMG-C7 cells transfected with zyxin siRNA or scramble RNA. After treatment with TGF-β1 for 24 h, total lysates were subjected to Western blot. GAPDH was used as a loading control. (B) Zyxin depletion abolished cell motility in TGF-β1-EMT. Cell motility was assessed by modified Boyden's chamber assay. NMuMG-C7 cells were transfected with zyxin siRNA or scramble RNA and treated or not with TGF-β1 for 24 h. The cells that migrated to the lower surface of the membrane were stained after 4 h of incubation. Scale bar, 250 μm. (C) The number of migrated cells in B. *p = 0.0344 versus Scramble RNA, TGF-β1 (−); **p = 0.0159 versus Scramble RNA, TGF-β1 (+). Results are shown as the mean ± SEM of four separate migration assays from two independent experiments. (D–K) Zyxin is essential for actin fiber formation in TGF-β1-EMT. Phalloidin staining was performed with NMuMG-C7 cells transfected with zyxin siRNA

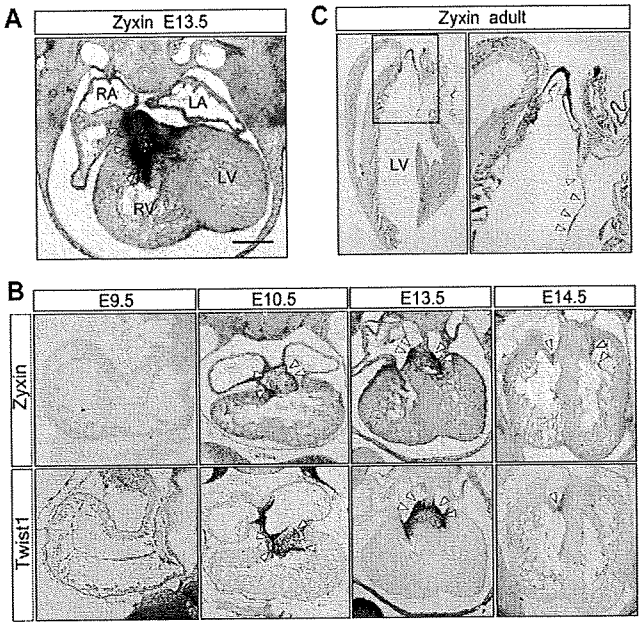

Figure 3. Zyxin is expressed in AVC during cardiac morphogenesis and valves in adult. (A) In situ hybridization for *zyxin* in E13.5 mouse embryo. Arrowheads indicate the strong expression of zyxin in AVC. RA, LA, RV, and LV stand for right atrium, left atrium, right ventricle, and left ventricle, respectively. Scale bar, 250 μm. (B) In situ hybridization for *zyxin* or *Twist1* from E9.5 to E14.5. Arrowheads indicate the expression of each gene. Note that the expression pattern of zyxin and Twist1 are highly correlated with each other. (C) In situ hybridization for *zyxin* in adult heart. The black square indicates the region of higher magnification shown to the right. Arrowhead indicates the zyxin expression in the mitral valve.

of cells (Figure 4D, Migratory), only 22% of the shZyxin-transduced explants exhibited endocardial cell migration and the majority remained cobblestone-like appearance (Figure 4D, Nonmigratory).

Invasiveness into extracellular matrices is an important feature for the endocardial cells that undergo EMT, because it is required for the endocardial cushion cellularization (Niessen *et al.*, 2008). Therefore, we examined the invasiveness of the explanted endocardial cells into collagen gel by confocal microscopy. Consequently, invasion of the zyxin-depleted cells was significantly reduced compared with the control cells (Figure 4E). Finally, the effect of zyxin depletion on actin fiber formation was addressed in the explanted cells. Although the prominent actin stress fiber formation was observed in shLacZ-transduced explants (Figure 4F, LacZ shRNA), only scarce actin network formation was seen in the shZyxin-transduced explants (Figure 4F, zyxin shRNA). These findings suggest that zyxin contributes to the endocardial EMT by regulating cell motility though the reorganization of actin fibers.

Twist1 Regulates Zyxin in TGF-β1-EMT

To clarify how zyxin expression is regulated during EMT, we tested the potential transcription factors that are reported to promote EMT (Thuault *et al.*, 2006). NMuMG-C7 cells expressed Twist1, Twist2, TwistNB, Snail, and HMGA2 (Figure 5A). Among them, the expression of Twist1 and Snail was increased by TGF-β1 treatment (Figure 5A). Subsequently, we transduced NMuMG-C7 cells with retrovirus vectors expressing Snail, Twist1, HMGA2 (Thuault *et al.*, 2006), or control EGFP. Among them, Twist1 up-regulated zyxin mRNA (Figure 5B) and induced zyxin expression (Figure 5C). These results suggest that Twist1 can promote zyxin expression. We then studied the requirement of Twist1 for zyxin up-regulation by TGF-β1. On knockdown of Twist1 (Figure 5D), TGF-β1 failed to up-regulate zyxin mRNA (Figure 5E) and to induce the expression of zyxin (Figure 5, F and G). Twist1 knockdown also decreased the basal expression of zyxin, suggesting the contribution of Twist1 to the basal expression of zyxin (Figure 5, F and G). We then studied whether focal adhesion-related proteins were generally regulated by TGF-β1 or Twist1. We investigated the expression of paxillin, FAK, vinculin, and p130Cas. Among them, paxillin was up-regulated by TGF-β1 (Supplementary Figure S5A). Twist1 depletion by siTwist1, however, did not abrogate the up-regulation of paxillin by TGF-β1 (Supplementary Figure S5B). These results suggest that focal adhesion proteins are not generally regulated by a single transcription factor in TGF-β1–induced EMT. Next, we investigated the possibility that paxillin was regulated by Snail, which was up-regulated by TGF-β1 (Figure 5A). We found paxillin was not up-regulated by Snail, either (Supplementary Figure S5C). These results delineate the signaling pathway, TGF-β1-Twist1-zyxin in the EMT and raise the possibility that different sets of focal adhesion proteins are regulated by distinct transcription factors.

Twist1 Uses Zyxin to Execute EMT

Twist1 is a potent EMT inducer, the function of which is well-characterized in cancer metastasis (Ansieau *et al.*, 2008). We explored whether zyxin is required for Twist1-induced EMT. NMuMG-C7 cells transduced with Twist1 (NMuMG-Twist1) underwent EMT and exhibited cell scattering, numerous protrusions (Figure 6A, arrowhead) and stress fiber formation (Figure 6C). In contrast, NMuMG-Twist1 cells transfected with zyxin siRNA exhibited fewer protrusions and rectangular cell morphology (Figure 6B). Actin stress fiber formation was also attenuated (Figure 6D). These findings suggest that zyxin is required for the cell shape change and actin fiber formation induced by Twist1. In addition, although NMuMG-Twist1 cells displayed enhanced migratory activity, depletion of zyxin strongly suppressed the migration of NMuMG-Twist1 cells (Figure 6, E and F). These results suggest that Twist1 induces EMT by up-regulating zyxin and by potential zyxin-dependent effects on actin reorganization to promote cell migration.

Thus, zyxin plays a significant role in motility acquisition in EMT by promoting actin fiber formation and confers the

Figure 2 (cont). or scramble RNA and treated or not with TGF-β1 for 24 h. Apical and basal actin network were observed separately with a confocal microscope. Note that both the apical and basal actin fiber formation were hampered by zyxin depletion. Scale bar, 50 μm. (L) The scheme of EGFP-tagged zyxin deletion constructs. EGFP–zyxin constructs were introduced into NMuMG-C7 cells by transient transfection. FL: full length. (M) NMuMG-C7 cells were transduced with lentivirus vector that expresses shZyxin that targets 3′UTR. The resultant cells were then transfected with the EGFP–zyxin constructs that lack 3′UTR. The suppression of endogenous zyxin and the expression of transfected genes were confirmed by blotting with anti-zyxin and ant-EGFP antibodies. LIM only construct lacks the epitope recognized by zyxin antibody. (N) Neither ΔLIM nor LIM only constructs rescued the endogenous zyxin depletion. Endogenous zyxin-depleted cells were transfected with EGFP–zyxin constructs and treated with TGF-β1 for 24 h. Actin fiber formation was observed in the cells transfected with FL (arrowhead), but not with ΔLIM or LIM only constructs. Scale bar, 50 μm.

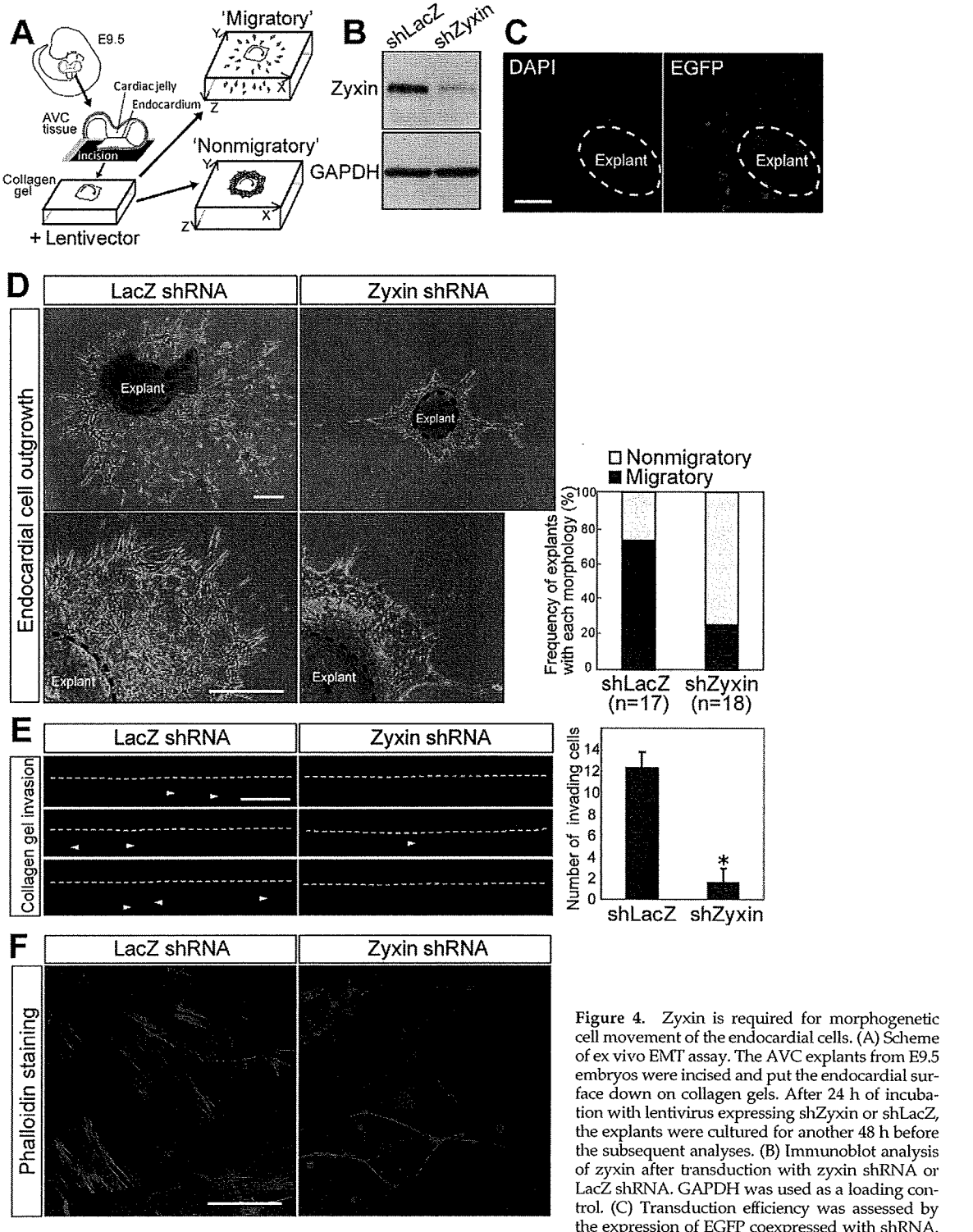

Figure 4. Zyxin is required for morphogenetic cell movement of the endocardial cells. (A) Scheme of ex vivo EMT assay. The AVC explants from E9.5 embryos were incised and put the endocardial surface down on collagen gels. After 24 h of incubation with lentivirus expressing shZyxin or shLacZ, the explants were cultured for another 48 h before the subsequent analyses. (B) Immunoblot analysis of zyxin after transduction with zyxin shRNA or LacZ shRNA. GAPDH was used as a loading control. (C) Transduction efficiency was assessed by the expression of EGFP coexpressed with shRNA. After 48 h of incubation after transduction, the explants were stained with DAPI and subjected to fluorescent microscopy. Scale bar, 100 μm. (D) Depletion of zyxin abolished the outgrowth of the endocardial cells. Phase-contrast images of AVC explants after 48 h of incubation after transduction. Scale bars, 250 μm. Right graph shows the proportion of colonies with the morphology defined by criteria described in *Materials and Methods*. (E) Cell invasiveness was suppressed by zyxin depletion. Collagen gel invasiveness assessed by XZ confocal microscopy. After 48 h of incubation after transduction, the explants were fixed and stained with DAPI. Broken lines indicate the surface of the gel. Scale bar, 100 μm. Right panel shows the number of the cells invading into the gel per unit area presented as mean ± SEM (n = 6). *p = 0.0048 versus shLacZ. (F) Zyxin is required for actin fiber reorganization in the endocardial cells. After 48 h of incubation after transduction, the explants were fixed and stained with phalloidin and DAPI and subjected to confocal microscopy. Note the decreased actin stress fibers in the endocardial cells that underwent EMT upon the collagen gel. Scale bar, 50 μm.

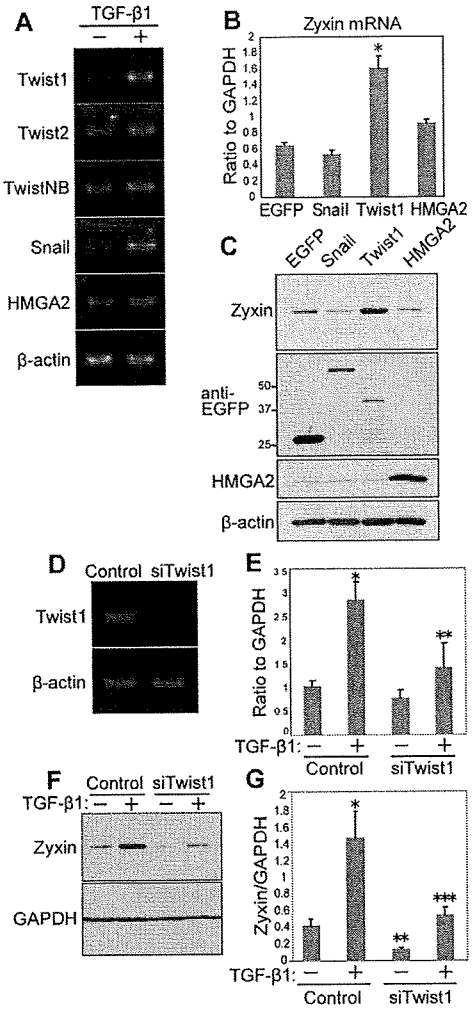

Figure 5. Twist1 regulates zyxin in TGF-β1-EMT. (A) Expression analysis of EMT inducers in NMuMG-C7 cells. RT-PCR performed with total RNA isolated from NMuMG-C7 cells treated with or without TGF-β1. β-Actin was used as a control. (B) Twist1 up-regulates zyxin. Real-time PCR performed with total RNA from NMuMG-C7 cells transduced with EGFP, Snail, Twist1, or HMGA2. *p = 0.0122 versus EGFP. Error bars, the SEM of three technical replicates. (C) Twist1 induced the expression of zyxin. Immunoblot analysis of zyxin in NMuMG-C7 cells transduced with EGFP, EGFP-Snail, EGFP-Twist1, or HMGA2. The expression of transduced genes was confirmed by blotting with anti-EGFP and anti-HMGA2 antibodies. (D) Efficacy of Twist1 RNAi assessed by RT-PCR. Total RNA from NMuMG-C7 cells transfected with either Twist1 siRNA or scramble RNA were subjected to RT-PCR. (E) Twist1 depletion abrogated up-regulation of zyxin by TGF-β1. Real-time PCR analysis of zyxin mRNA in NMuMG-C7 cells transfected with Twist1 siRNA or scramble RNA and treated or not with TGF-β1. Results are shown as the mean ± SEM (n = 3). *p = 0.011 when compared with control, TGF-β1(−); **p = 0.0236 when compared with control, TGF-β1(+). (F) Twist1 depletion suppressed the expression of zyxin. Immunoblot analysis of zyxin in NMuMG-C7 cells transfected with Twist1 siRNA or scramble RNA and treated or not with TGF-β1. GAPDH was used as a loading control. (G) Results of F were quantitated by densitometry using NIH ImageJ. Error bars, SD from triplicate experiments. *p = 0.0084 when compared with control, TGF-β1(−); **p = 0.035 when compared with control, TGF-β1(−); ***p = 0.012 when compared with control, TGF-β1(+).

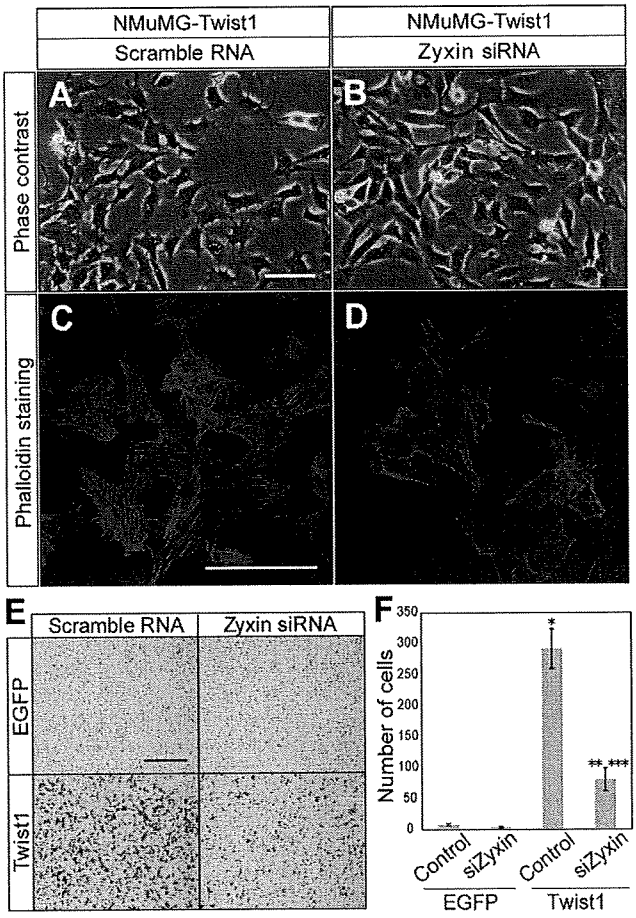

Figure 6. Twist1 uses zyxin to execute EMT. (A and B) Twist1-induced cell morphological change was abrogated by zyxin depletion. NMuMG-C7 cells transduced with Twist1 were transfected with zyxin siRNA or scramble RNA. Phase-contrast microscopy was done 48 h after transfection. (A) Arrowheads indicate the cell protrusions induced by Twist1 transduction. Scale bar, 100 μm. (C and D) Twist1-induced actin fiber reorganization was abrogated by zyxin depletion. Phalloidin staining in NMuMG-Twist1 cells transfected with zyxin siRNA or scramble RNA. Scale bar, 100 μm. (E) Modified Boyden's chamber assay performed with NMuMG-Twist1 cells transfected with zyxin siRNA or scramble RNA. After incubation for 4 h, the cells that migrated to the lower surface of the membrane were stained. Scale bar, 250 μm. (F) The number of migrated cells in E. *p = 0.0013 versus NMuMG-EGFP, Control; **p = 0.0144 versus NMuMG-Twist1, Control; ***p = 0.0184 versus NMuMG-EGFP, Control. Results are shown as the mean ± SEM of four separate migration assays from two independent experiments.

endocardial cells the motility required for cardiac morphogenesis.

DISCUSSION

We delineate the signaling pathway, TGF-β1-Twist1-zyxin, in the EMT in cultured cells and demonstrate the involvement of this signaling in valvulogenesis in the development of the heart in vivo. Depletion of zyxin abrogated either Twist1-dependent or TGF-β1–dependent EMT in NMuMG cells, confirming this signaling.

We show that zyxin is essential for cell migration and actin fiber reorganization in TGF-β1-EMT. Zyxin and paxil-

lin are the prototypes of two related subfamilies of LIM domain proteins that are localized primarily at focal adhesion plaques (Wang and Gilmore, 2003). Although paxillin and Hic-5 are required for the progression of EMT (Tumbarello *et al.*, 2005), the involvement of zyxin in EMT has not been reported. On EMT induction, zyxin mobilized from focal adhesions to actin stress fibers. Although our findings are based on EGFP-fusion protein study, EGFP-tagged zyxin was reported to display a distribution pattern that is indistinguishable from that of the endogenous zyxin (Nix *et al.*, 2001; Hotulainen and Lappalainen, 2006). Mechanostress-induced relocation of zyxin has been reported (Yoshigi *et al.*, 2005). Yoshigi *et al.* showed that cyclic stretch or sheer stress to cells in vitro resulted in mobilization of zyxin from focal adhesions to actin filaments. Lele *et al.* (2006) measured the molecular binding kinetics of focal adhesion proteins in living cells using modified fluorescence recovery after photobleaching technique and showed mechanical forces specifically altered the molecular binding kinetics of zyxin, but not of vinculin. What role does the relocation of zyxin play, if any, in endocardial morphogenesis? Yashiro *et al.* (2007) has shown that left-right asymmetry of aortic arch was determined by asymmetric blood flow during the development of great arteries. Similarly, sheer stress induced by blood flow or mechanostress altered through cardiac morphogenesis might induce the relocation of proteins that sense mechanical forces, thereby contributing to endocardial morphogenesis. The significance of relocation requires further analysis, although it is speculated that zyxin interacts with a set of proteins such as VASP (Yoshigi *et al.*, 2005) as an adaptor protein on the actin stress fibers. The cells transfected with zyxin siRNA failed to show TGF-β1–enhanced cell motility and fiber formation, indicating that zyxin is essential for motility acquisition and actin fiber reorganization induced by TGF-β1 in NMuMG cells.

We delineated the signaling pathway, TGF-β1-Twist1-zyxin in EMT. TGF-β1 induced the expression of Twist1 and Snail. Twist1, but not Snail, was required for the up-regulation of zyxin by TGF-β1. Numerous focal adhesion proteins are regulated in EMT (Zavadil and Bottinger, 2005). In NMuMG-C7 cells, paxillin was up-regulated by TGF-β1 (Supplementary Figure S5A), but neither Twist1 nor Snail induced paxillin expression, suggesting the other transcription factor was responsible for it. It is of note that Twist1 or Snail targets different genes despite that both are potent EMT inducers. These results implied the multiple layers of transcriptional regulation in EMT. Coordinated expression of transcription factors might be important for the efficient progression of EMT. Niessen *et al.* showed that Snail and Slug, which belong to the same protein family, are regulated differentially and function in combination during AVC morphogenesis (Niessen *et al.*, 2008). Thuault *et al.* (2006) showed that HMGA2 induces the expression of Snail/Slug and weakly of Twist1 in TGF-β1–induced EMT. These reports support that EMT is more efficiently executed by coordination of multiple transcriptional regulations. Further investigation is necessary to address how the cellular phenomena are regulated by multiple layers of transcriptional regulation.

Twist1 is an EMT regulator well characterized in cancer metastasis (Yang *et al.*, 2004). It is of note that Twist1 uses zyxin to induce the cell morphological change and migration. Therefore, zyxin might be a target of treatment or prevention for cancer metastasis. We confirmed the presence of several E-box sites, which basic helix-loop-helix transcription factors including Twist1 preferentially bind to, in the promoter region of zyxin gene. Further analysis is needed to reveal how Twist1 promotes transcription of zyxin.

We revealed that zyxin was predominantly expressed in AVC in the embryonic heart undergoing EMT and that zyxin was required for migration and actin fiber reorganization in the endocardial cells. The expression of zyxin mRNA began at E10.5 that corresponds to the onset of endocardial EMT and became predominant in AVC of developing heart and in adult valves. The expression of Twist1 in AVC was highly correlated with that of zyxin. TGF-β1 is expressed in AVC and contributes to valvulogenesis (Nakajima *et al.*, 2000; Molin *et al.*, 2003), suggesting functional coordination of TGF-β1-Twist1-zyxin pathway in vivo. Most recently, the role for Twist1 in AVC development was reported (Shelton and Yutzey, 2008), and further molecular dissection would lead to better understanding of cardiac morphogenesis.

We further examined the importance of zyxin in EMT by ex vivo assay using E9.5 AVC tissue explants. The endocardial cells transduced with lentivirus vector expressing zyxin shRNA failed to exhibit outgrowth and invasiveness into collagen gels and to execute actin fiber reorganization. Together, zyxin is essential for the endocardial cells to undergo EMT in which zyxin promotes cell migration through actin fiber reorganization. Although zyxin-null mice are viable and fertile (Hoffman *et al.*, 2003), the hearts of the zyxin-null mice have not been inspected in detail. We considered two possibilities for no phenotype in zyxin-null mice. First, the abnormalities might be minor ones requiring careful observation, such as bicuspid aortic valves (Garg *et al.*, 2005) or malformation of supporting apparatus such as chordae tendineae (Norris *et al.*, 2008). Second, there might be genetic redundancy and chronic loss of zyxin might be overcome. To support this, although single knockout mice of VASP, with which zyxin directly interacts, exhibit no cardiac phenotype, but triple knockout mice of VASP, Ena and Ena-VASP-like show abnormally thin endocardium (Furman *et al.*, 2007). It might be necessary to ablate plural genes including LIM-family proteins to observe abnormal phenotypes due to the absence of zyxin. In *Xenopus laevis*, Martynova *et al.* (2008) revealed that zyxin expression increased along gastrulation that is another example of developmental EMT, and administration of zyxin morpholino resulted in disruption of embryos during gastrulation. It implied the essential role for zyxin in EMT during gastrulation. Thus, considering the particularly strong expression of zyxin in AVC undergoing EMT and the result from ex vivo AVC explant assay, we conclude that zyxin is required for migration and actin fiber reorganization of the endocardial cells.

In this study, we delineate the essential signaling, TGF-β1-Twist1-zyxin pathway, in in vitro EMT using cultured cells and in vivo EMT using the developing heart.

ACKNOWLEDGMENTS

We thank Tsuyoshi Akagi for providing pCX4 vectors. This work was supported by grants from the Ministry of Education, Culture, Sports, Science and Technology, Japan Heart Association, and Miyata Heart Foundation.

REFERENCES

Akagi, T., Sasai, K., and Hanafusa, H. (2003). Refractory nature of normal human diploid fibroblasts with respect to oncogene-mediated transformation. Proc. Natl. Acad. Sci. USA. *100*, 13567–13572.

Ansieau, S., *et al.* (2008). Induction of EMT by twist proteins as a collateral effect of tumor-promoting inactivation of premature senescence. Cancer Cell *14*, 79–89.

Bartram, U., Molin, D. G., Wisse, L. J., Mohamad, A., Sanford, L. P., Doetschman, T., Speer, C. P., Poelmann, R. E., and Gittenberger-de Groot, A. C. (2001). Double-outlet right ventricle and overriding tricuspid valve reflect disturbances of looping, myocardialization, endocardial cushion differentiation, and apoptosis in TGF-beta(2)-knockout mice. Circulation *103*, 2745–2752.

Beckerle, M. C. (1998). Spatial control of actin filament assembly: lessons from *Listeria*. Cell *95*, 741–748.

Bruneau, B. G. (2008). The developmental genetics of congenital heart disease. Nature *451*, 943–948.

Camenisch, T. D., Molin, D. G., Person, A., Runyan, R. B., Gittenberger-de Groot, A. C., McDonald, J. A., and Klewer, S. E. (2002). Temporal and distinct TGFbeta ligand requirements during mouse and avian endocardial cushion morphogenesis. Dev. Biol. *248*, 170–181.

Cano, A., Perez-Moreno, M. A., Rodrigo, I., Locascio, A., Blanco, M. J., del Barrio, M. G., Portillo, F., and Nieto, M. A. (2000). The transcription factor snail controls epithelial-mesenchymal transitions by repressing E-cadherin expression. Nat. Cell Biol. *2*, 76–83.

Chang, C. P., Neilson, J. R., Bayle, J. H., Gestwicki, J. E., Kuo, A., Stankunas, K., Graef, I. A., and Crabtree, G. R. (2004). A field of myocardial-endocardial NFAT signaling underlies heart valve morphogenesis. Cell *118*, 649–663.

Fradelizi, J., Noireaux, V., Plastino, J., Menichi, B., Louvard, D., Sykes, C., Golsteyn, R. M., and Friederich, E. (2001). ActA and human zyxin harbour Arp2/3-independent actin-polymerization activity. Nat. Cell Biol. *3*, 699–707.

Furman, C., Sieminski, A. L., Kwiatkowski, A. V., Rubinson, D. A., Vasile, E., Bronson, R. T., Fassler, R., and Gertler, F. B. (2007). Ena/VASP is required for endothelial barrier function in vivo. J. Cell Biol. *179*, 761–775.

Garg, V., Muth, A. N., Ransom, J. F., Schluterman, M. K., Barnes, R., King, I. N., Grossfeld, P. D., and Srivastava, D. (2005). Mutations in NOTCH1 cause aortic valve disease. Nature *437*, 270–274.

Hayashi, M., Nimura, K., Kashiwagi, K., Harada, T., Takaoka, K., Kato, H., Tamai, K., and Kaneda, Y. (2007). Comparative roles of Twist-1 and Id1 in transcriptional regulation by BMP signaling. J. Cell Sci. *120*, 1350–1357.

Hetey, S. E., Lalonde, D. P., and Turner, C. E. (2005). Tyrosine-phosphorylated Hic-5 inhibits epidermal growth factor-induced lamellipodia formation. Exp. Cell Res. *311*, 147–156.

Hoffman, L. M., *et al.* (2003). Targeted disruption of the murine zyxin gene. Mol. Cell Biol. *23*, 70–79.

Hotulainen, P., and Lappalainen, P. (2006). Stress fibers are generated by two distinct actin assembly mechanisms in motile cells. J. Cell Biol. *173*, 383–394.

Kadrmas, J. L., and Beckerle, M. C. (2004). The LIM domain: from the cytoskeleton to the nucleus. Nat. Rev. Mol. Cell Biol. *5*, 920–931.

Koibuchi, N., and Chin, M. T. (2007). CHF1/Hey2 plays a pivotal role in left ventricular maturation through suppression of ectopic atrial gene expression. Circ. Res. *100*, 850–855.

Lele, T. P., Pendse, J., Kumar, S., Salanga, M., Karavitis, J., and Ingber, D. E. (2006). Mechanical forces alter zyxin unbinding kinetics within focal adhesions of living cells. J. Cell Physiol. *207*, 187–194.

Lowry, O. H., Rosebrough, N. J., Farr, A. L., and Randall, R. J. (1951). Protein measurement with the Folin phenol reagent. J. Biol. Chem. *193*, 265–275.

Ma, L., Lu, M. F., Schwartz, R. J., and Martin, J. F. (2005). Bmp2 is essential for cardiac cushion epithelial-mesenchymal transition and myocardial patterning. Development *132*, 5601–5611.

Martynova, N. Y., Eroshkin, F. M., Ermolina, L. V., Ermakova, G. V., Korotaeva, A. L., Smurova, K. M., Gyoeva, F. K., and Zaraisky, A. G. (2008). The LIM-domain protein zyxin binds the homeodomain factor Xanf1/Hesx1 and modulates its activity in the anterior neural plate of *Xenopus laevis* embryo. Dev. Dyn. *237*, 736–749.

Miettinen, P. J., Ebner, R., Lopez, A. R., and Derynck, R. (1994). TGF-beta induced transdifferentiation of mammary epithelial cells to mesenchymal cells: involvement of type I receptors. J. Cell Biol. *127*, 2021–2036.

Molin, D. G., Bartram, U., Van der Heiden, K., Van Iperen, L., Speer, C. P., Hierck, B. P., Poelmann, R. E., and Gittenberger-de-Groot, A. C. (2003). Expression patterns of Tgfbeta1–3 associate with myocardialisation of the outflow tract and the development of the epicardium and the fibrous heart skeleton. Dev. Dyn. *227*, 431–444.

Nakajima, Y., Yamagishi, T., Hokari, S., and Nakamura, H. (2000). Mechanisms involved in valvuloseptal endocardial cushion formation in early cardiogenesis: roles of transforming growth factor (TGF)-beta and bone morphogenetic protein (BMP). Anat. Rec. *258*, 119–127.

Nakaya, Y., Sukowati, E. W., Wu, Y., and Sheng, G. (2008). RhoA and microtubule dynamics control cell-basement membrane interaction in EMT during gastrulation. Nat. Cell Biol. *10*, 765–775.

Niessen, K., Fu, Y., Chang, L., Hoodless, P. A., McFadden, D., and Karsan, A. (2008). Slug is a direct Notch target required for initiation of cardiac cushion cellularization. J. Cell Biol. *182*, 315–325.

Nix, D. A., Fradelizi, J., Bockholt, S., Menichi, B., Louvard, D., Friederich, E., and Beckerle, M. C. (2001). Targeting of zyxin to sites of actin membrane interaction and to the nucleus. J. Biol. Chem. *276*, 34759–34767.

Norris, R. A., Moreno-Rodriguez, R. A., Sugi, Y., Hoffman, S., Amos, J., Hart, M. M., Potts, J. D., Goodwin, R. L., and Markwald, R. R. (2008). Periostin regulates atrioventricular valve maturation. Dev. Biol. *316*, 200–213.

Perez-Moreno, M., Jamora, C., and Fuchs, E. (2003). Sticky business: orchestrating cellular signals at adherens junctions. Cell *112*, 535–548.

Runyan, R. B., and Markwald, R. R. (1983). Invasion of mesenchyme into three-dimensional collagen gels: a regional and temporal analysis of interaction in embryonic heart tissue. Dev. Biol. *95*, 108–114.

Saito, Y., *et al.* (2006). Transfection of human hepatocyte growth factor gene ameliorates secondary lymphedema via promotion of lymphangiogenesis. Circulation *114*, 1177–1184.

Sanford, L. P., Ormsby, I., Gittenberger-de Groot, A. C., Sariola, H., Friedman, R., Boivin, G. P., Cardell, E. L., and Doetschman, T. (1997). TGFbeta2 knockout mice have multiple developmental defects that are non-overlapping with other TGFbeta knockout phenotypes. Development *124*, 2659–2670.

Schneichel, K. L., and Beckerle, M. C. (1994). The LIM domain is a modular protein-binding interface. Cell *79*, 211–219.

Shelton, E. L., and Yutzey, K. E. (2008). Twist1 function in endocardial cushion cell proliferation, migration, and differentiation during heart valve development. Dev. Biol. *317*, 282–295.

Sridurongrit, S., Larsson, J., Schwartz, R., Ruiz-Lozano, P., and Kaartinen, V. (2008). Signaling via the Tgf-beta type I receptor Alk5 in heart development. Dev. Biol. *322*, 208–218.

Sung, S. Y., Hsieh, C. L., Wu, D., Chung, L. W., and Johnstone, P. A. (2007). Tumor microenvironment promotes cancer progression, metastasis, and therapeutic resistance. Curr. Probl. Cancer *31*, 36–100.

Thiery, J. P. (2003). Epithelial-mesenchymal transitions in development and pathologies. Curr. Opin. Cell Biol. *15*, 740–746.

Thuault, S., Valcourt, U., Petersen, M., Manfioletti, G., Heldin, C. H., and Moustakas, A. (2006). Transforming growth factor-beta employs HMGA2 to elicit epithelial-mesenchymal transition. J. Cell Biol. *174*, 175–183.

Tumbarello, D. A., Brown, M. C., Hetey, S. E., and Turner, C. E. (2005). Regulation of paxillin family members during epithelial-mesenchymal transformation: a putative role for paxillin delta. J. Cell Sci. *118*, 4849–4863.

Vasioukhin, V., Bauer, C., Yin, M., and Fuchs, E. (2000). Directed actin polymerization is the driving force for epithelial cell-cell adhesion. Cell *100*, 209–219.

Wang, Y., and Gilmore, T. D. (2003). Zyxin and paxillin proteins: focal adhesion plaque LIM domain proteins go nuclear. Biochim. Biophys. Acta *1593*, 115–120.

Yang, J., *et al.* (2004). Twist, a master regulator of morphogenesis, plays an essential role in tumor metastasis. Cell *117*, 927–939.

Yashiro, K., Shiratori, H., and Hamada, H. (2007). Haemodynamics determined by a genetic programme govern asymmetric development of the aortic arch. Nature *450*, 285–288.

Yonemura, S., Itoh, M., Nagafuchi, A., and Tsukita, S. (1995). Cell-to-cell adherens junction formation and actin filament organization: similarities and differences between non-polarized fibroblasts and polarized epithelial cells. J. Cell Sci. *108*(Pt 1), 127–142.

Yoshigi, M., Hoffman, L. M., Jensen, C. C., Yost, H. J., and Beckerle, M. C. (2005). Mechanical force mobilizes zyxin from focal adhesions to actin filaments and regulates cytoskeletal reinforcement. J. Cell Biol. *171*, 209–215.

Zavadil, J., and Bottinger, E. P. (2005). TGF-beta and epithelial-to-mesenchymal transitions. Oncogene *24*, 5764–5774.

Molecular Biology of the Cell
Vol. 20, 1949–1959, April 1, 2009

EphA2 Engages Git1 to Suppress Arf6 Activity Modulating Epithelial Cell–Cell Contacts

Koichi Miura,*† Jin-Min Nam,*‡ Chie Kojima,*‡ Naoki Mochizuki,† and Hisataka Sabe*‡

*Department of Molecular Biology, Osaka Bioscience Institute, Suita, Osaka 565-0874, Japan; ‡Graduate School of Biostudies, Kyoto University, Kyoto 606-8502, Japan; and †Department of Structural Analysis, National Cardiovascular Center Research Institute, Suita, Osaka 565-8565, Japan

Submitted June 2, 2008; Revised January 23, 2009; Accepted January 27, 2009
Monitoring Editor: J. Silvio Gutkind

ADP-ribosylation factor (Arf) 6 activity is crucially involved in the regulation of E-cadherin–based cell–cell adhesions. Erythropoietin-producing hepatocellular carcinoma (Eph)-family receptors recognize ligands, namely, ephrins, anchored to the membrane of apposing cells, and they mediate cell–cell contact-dependent events. Here, we found that Arf6 activity is down-regulated in Madin-Darby canine kidney cells, which is dependent on cell density and calcium ion concentration, and we provide evidence of a novel signaling pathway by which ligand-activated EphA2 suppresses Arf6 activity. This EphA2-mediated suppression of Arf6 activity was linked to the induction of cell compaction and polarization, but it was independent of the down-regulation of extracellular signal-regulated kinase 1/2 kinase activity. We show that G protein-coupled receptor kinase-interacting protein (Git) 1 and noncatalytic region of tyrosine kinase (Nck) 1 are involved in this pathway, in which ligand-activated EphA2, via its phosphorylated Tyr594, binds to the Src homology 2 domain of Nck1, and then via its Src homology 3 domain binds to the synaptic localizing domain of Git1 to suppress Arf6 activity. We propose a positive feedback loop in which E-cadherin–based cell–cell contacts enhance EphA-ephrinA signaling, which in turn down-regulates Arf6 activity to enhance E-cadherin–based cell–cell contacts as well as the apical-basal polarization of epithelial cells.

INTRODUCTION

E-cadherin–mediated cell–cell adhesion is essential for the integrity of epithelial cell layers, as well as their normal functions (Takeichi, 1991; Gumbiner, 2005). ADP-ribosylation factor (Arf) 6 primarily regulates recycling of plasma membrane components, as well as remodeling of the membrane and actin cytoskeleton at the cell peripheries via its GTPase cycle (Donaldson, 2003). It has been shown that expression of an inactive form of Arf6, Arf6T27N, blocks hepatocyte growth factor (HGF)-induced internalization of E-cadherin–based junctional components in Madin-Darby canine kidney (MDCK) epithelial cells, whereas expression of a constitutively active form of Arf6, Arf6Q67L, causes disassembly of adherens junctions (Palacios *et al.*, 2001, 2002). The results of small interfering RNA (siRNA)-mediated knockdown of GEP100, a guanine nucleotide exchanging factor for Arf6, also support a similar notion that inactivation of Arf6 renders resistance to HGF-induced disruption of adherens junctions of human epidermoid carcinoma CaSki cells (Hiroi *et al.*, 2006). Experiments using fetal hepatocyte cells prepared from *Arf6−/−* mice also support this notion (Suzuki *et al.*, 2006). Moreover, we have shown that activation of Arf6 by GEP100 plays a pivotal role in the invasive phenotypes of different breast cancer cells, which is accompanied by the disruption of E-cadherin–mediated cell–cell adhesion in breast cancer MCF7 cells (Morishige *et al.*, 2008). Therefore, down-regulation of Arf6 activity seems to be pivotal for the formation and maintenance of E-cadherin–mediated cell–cell adhesions. However, the mechanism by which Arf6 activity is suppressed in cell–cell contacts has not yet been identified.

Eph receptor tyrosine kinases are classified into either EphA or EphB subfamilies based on the identity of their ligands, ephrinA- and ephrinB-subfamily members, respectively, and both are anchored to the cell membrane by different mechanisms (Pasquale, 2005). Eph receptors and ephrins each have overlapping specificity: several receptors can bind to one ligand, and, in turn, several ligands can bind to one receptor (Pasquale, 2005). The physiological roles of Eph–ephrin interactions have been well characterized in the nervous system, such as during axon guidance and synapse formation, and also in somite and vascular development (Pasquale, 2005). Eph receptors, when ligand-activated, become tyrosine phosphorylated and evoke a variety of different intracellular signaling cascades, which mostly exert negative regulatory effects, such as on migration and proliferative signaling (Miao *et al.*, 2000, 2001, 2003; Noren *et al.*, 2006).

EphA2 is normally expressed at high levels in adult epithelial cells, as well as in restricted regions of the embryo

This article was published online ahead of print in *MBC in Press* (http://www.molbiolcell.org/cgi/doi/10.1091/mbc.E08-06-0549) on February 4, 2009.

Address correspondence to: Hisataka Sabe (sabe@obi.or.jp).

Abbreviations used: Arf, ADP-ribosylation factor; Eph, erythropoietin-producing hepatocellular carcinoma; GAP, GTPase-activating protein; Git, G protein-coupled receptor kinase-interacting protein; GGA, Golgi-localizing, gamma-adaptin ear domain homology, ARF-binding protein; HGF, hepatocyte growth factor; MDCK, Madin-Darby canine kidney; Nck, noncatalytic region of tyrosine kinase; SLD, synaptic localizing domain.

during early development (Ruiz and Robertson, 1994; Surawska *et al.*, 2004). EphA2 is frequently overexpressed in different types of human carcinomas, including those of the breast, lung, prostate, esophagus, and kidney (Surawska *et al.*, 2004). The *EphA2* gene is a direct transcription target of the Ras/Raf/mitogen-activated protein kinase kinase (Mek)/extracellular signal-regulated kinase (Erk)1/2 pathway (Macrae *et al.*, 2005). Overexpression of EphA2 in some carcinomas may hence merely be a result of the activation of this pathway in carcinomas rather than an etiologic event (Macrae *et al.*, 2005). In contrast, it has been demonstrated that stimulation of overexpressed EphA2 in some tumor cells by high concentrations of exogenous ligands can negatively regulate the growth, survival, migration, and invasion of these cells (Zelinski *et al.*, 2001; Noblitt *et al.*, 2004). Moreover, disruption of the *EphA2* gene in mice leads to increased susceptibility to skin carcinogenesis (Guo *et al.*, 2006), suggesting a tumor suppressing role of EphA2.

Here, we found that EphA2, when ligand activated, suppresses Arf6 activity. We show that EphA2 uses G protein-coupled receptor kinase-interacting protein (Git) 1 to suppress Arf6 activities. We describe the precise mechanism by which EphA2 is linked to Git1, and we demonstrate that this pathway acts to enhance E-cadherin–based cell–cell adhesions and the apical-basal polarization of epithelial cells.

MATERIALS AND METHODS

Cells

MDCK cells, obtained from Sh. Tsukita (Kyoto University), and human embryonic kidney (HEK) 293T cells were cultured as described previously (Mazaki *et al.*, 2001). Fetal calf serum was purchased from HyClone Laboratories (Logan, UT).

For the culture of MDCK cells under the "sparse density" and the "dense density," 1×10^6 and 5×10^6 cells, respectively, were seeded onto a Φ 90-mm plastic dish and cultured for a further 24 h before subjecting to analysis.

For ephrinA1 stimulation, cells were treated with nonclustered ephrinA1-Fc (R&D Systems, Minneapolis, MN) at 125 ng/ml or control Fc (R&D Systems) at 62.5 ng/ml for 30 min, unless otherwise indicated.

Antibodies and Chemicals

The rabbit polyclonal antibody against Git2 was generated as described previously (Mazaki *et al.*, 2001). Other antibodies were purchased from commercial sources: rat monoclonal antibodies against E-cadherin (clone ECCD-2, Takara, Kyoto, Japan; and clone DECMA-1, Sigma-Aldrich, St. Louis, MO); rabbit polyclonal antibody against Git1 (H-170; Santa Cruz Biotechnology, Santa Cruz, CA); EphA2 (C-20; Santa Cruz Biotechnology); zona occludens (ZO)-1 (Zymed Laboratories, South San Francisco, CA); Erk1/2 (Cell Signaling Technology, Danvers, MA); FLAG (Sigma-Aldrich); mouse monoclonal antibody (mAb) against Arf6 (3A-1; Santa Cruz Biotechnology); noncatalytic region of tyrosine kinase (Nck) (BD Biosciences, San Jose, CA); Ezrin (EZ-1; Biodesign International, Kennebunk, ME); phospho-Erk1/2 (Cell Signaling Technology), hemagglutinin (HA) (16B12; BAbCo, Richmond, CA); glutathione transferase (GST) (Millipore, Billerica, MA); FLAG (M2; Sigma-Aldrich); nonspecific rabbit and mouse immunoglobulin G (IgG) (Sigma-Aldrich); horseradish peroxidase-conjugated goat anti-rabbit or anti-mouse IgG; $F(ab')_2$ fragments of biotin-conjugated goat anti-rabbit or anti-mouse IgG (Jackson ImmunoResearch Laboratories, West Grove, PA); and Alexa-labeled goat anti-rabbit, anti-mouse, or anti-rat IgG (Invitrogen, Carlsbad, CA). All other chemical reagents were purchased from Sigma-Aldrich and Wako Pure Chemicals (Kyoto, Japan), unless otherwise stated.

Complementary DNAs (cDNAs)

cDNA encoding mouse Git1 was amplified by polymerase chain reaction (PCR) from mouse brain first-strand cDNA. Other cDNAs were provided by the following researchers: human EphA2 was from N. Mochizuki (National Cardiovascular Center, Osaka, Japan), mouse E-cadherin was from M. Takeichi (RIKEN CDB, Kobe, Japan); Venus was from A. Miyawaki (RIKEN BSI, Wako, Japan); mouse Arf1 and Arf6 were from K. Nakayama (Kyoto University), and mouse Nck1 was from T. Shishido (NAIST, Nara, Japan). pcDNA3 FLAG N dest, pcDNA3 HA N dest., and pEBG dest vectors were generated using the Gateway vector conversion kit (Invitrogen). EphA2, Git1, and Nck1 cDNAs were inserted into the pENTR/D topo vector and transferred into their destination vectors by using LR clonaseII (Invitrogen). pBabe puro Arf6-HA, Arf6T27N-HA, Arf6Q67L-HA, and Arf1Q71L-HA were generated by cloning HindIII-XbaI fragments from pcDNA3 Arf6-HA, Arf6T27N-HA, Arf6Q67L-HA, and Arf1Q71L-HA into the SnaBI site of the pBabe puro vector after filling of the ends. pVenus N1 E-cadherin was described previously (Bauer *et al.*, 2008).

Transfections

cDNA transfections were performed using Lipofectamine 2000 (Invitrogen) according to the manufacturer's instructions.

To establish cells stably expressing specific cDNAs, transfection-positive cells were selected by culturing in the presence of the appropriate drugs (4 μg/ml puromycin for the pBabe puro vector or 1 mg/ml G418 for the pcDNA3 and pVenus N1 vectors). Cells were then cloned by limited dilution, and the results were confirmed by at least two independent cell clones for each plasmid.

Small Interfering RNAs

MDCK cells were transfected with oligonucleotide duplexes by using a reverse transfection method, according to the manufacturer's instructions (Invitrogen). Briefly, cells were trypsinized, washed, and suspended in DMEM with 10% fetal calf serum. Then, they were plated onto a plastic dish in the presence of 10 nM oligonucleotide duplexes and Lipofectamine 2000 in Opti-MEM (Invitrogen), Finally, they were incubated for 48 h before being subjected to analysis. Nucleotide sequences used were as follows: for *Git1*, sense 5′-GAGGUGGAUAGAAGAGAAAAU-3′; and for *Nck1*, sense 5′-UCCUGGUGGCGAGUUCGAA-3′. An siRNA duplex with an irrelevant sequence (5′-GCGCGCUUUGUAGGAUUCG-3′) was purchased from Dharmacon RNA Technologies (Lafayette, CO).

For the rescue experiment of the Git1 siRNA treatment, mouse Git1 cDNA, tagged with FLAG, in which the siRNA target sequence was mutated into 5′-GAAGTGGATCGGCGGGAGAAC-3′ was used.

Calcium Switch

Calcium switch was performed according to the method described previously (Zantek *et al.*, 1999). Briefly, 8 mM EGTA was added to MDCK cells cultured at the dense density, and then cells were incubated for a further 30 min at 37°C. The medium was then exchanged with DMEM supplemented with 10% fetal calf serum and 4 mM $CaCl_2$, and cells were further incubated for the times indicated.

GST-Golgi-localizing, Gamma-Adaptin Ear Domain Homology, ARF-binding Protein (GGA) Pulldown, Immunoprecipitation, and Immunoblotting

Arf6 activities were measured using GST-GGA (Santy and Casanova, 2001). Cells were lysed in a lysis buffer (1% Triton X-100, 0.05% sodium cholate, 0.005% SDS, 50 mM Tris-HCl, pH 8.0, 100 mM NaCl, 10 mM $MgCl_2$, 10% glycerol, 2 mM dithiothreitol, 1 mM phenylmethylsulfonyl fluoride, 5 μg/ml aprotinin, 2 μg/ml leupeptin, and 3 μg/ml pepstatin A). After clarifying by centrifugation at 1500 $\times$ *g* for 5 min, supernatants were incubated with GST-GGA3 conjugated to glutathione-Sepharose for 40 min at 4°C.

Immunoprecipitation assays were performed using antibodies coupled with protein G-Sepharose, as described previously (Morishige *et al.*, 2008), in which cells were lysed in NP-40 buffer (1% Nonidet P-40, 20 mM Tris-HCl, pH 7.4, 150 mM NaCl, 5 mM EDTA, 1 mM Na_3VO_4, 1 mM phenylmethylsulfonyl fluoride, 5 μg/ml aprotinin, 2 μg/ml leupeptin, and 3 μg/ml pepstatin A). When cells were pretreated with ephrinA1-Fc or control Fc, biotin-conjugated $F(ab')_2$ fragments of goat anti-rabbit or anti-mouse IgG, coupled to streptavidin-Sepharose beads, were used. Three hundred micrograms of cell lysates was used for each GGA pulldown and immunoprecipitation.

Immunoblotting was performed as described previously (Morishige *et al.*, 2008). To enhance the signal from the endogenous Arf6 protein, Can Get Signal (Toyobo Engineering, Osaka, Japan) was used to dilute the anti-Arf6 antibody.

Immunofluorescence Microscopy

Acquisition of confocal images of cells was performed using confocal laser scanning microscopes (LSM510, Carl Zeiss, Jean, Germany and FV1000, Olympus, Tokyo, Japan), as described previously (Mazaki *et al.*, 2001). Z-sections were obtained at 0.5-μm step size. Focuses adjusted across the center of the majority of cell bodies were used to show the localization of E-cadherin, EphA2, Git1-FLAG, Arf-HA, and F-actin. To show the localization of ZO-1, projection images made by summing up all confocal sections into one image were used. Each figure of microscopic analysis shows representative results observed in at least three independent experiments.

RESULTS

Cell Density- and Calcium-dependent Suppression of Arf6 Activity

We first found that the cellular activities of Arf6, measured by the GST-GGA pulldown method (Santy and Casanova,

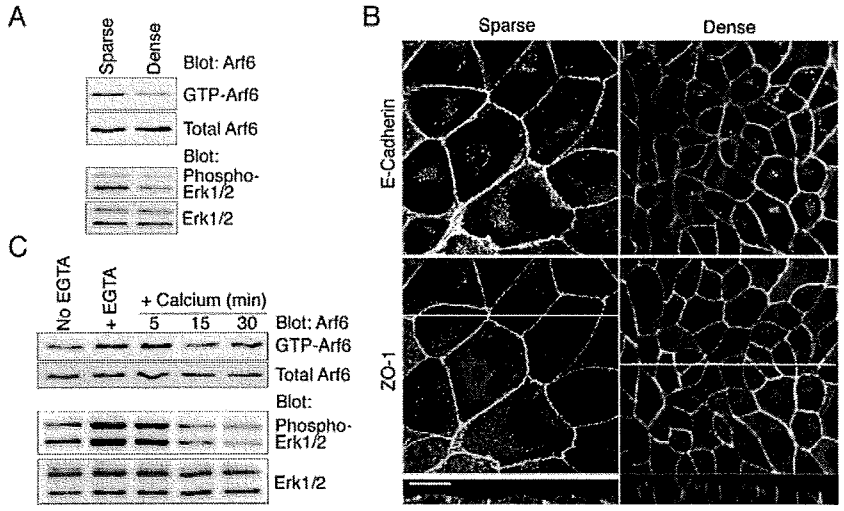

Figure 1. Cell density- and calcium-dependent suppression of Arf6 and Erk1/2 activities in MDCK cells. (A) Arf6 and Erk1/2 activities in cells cultured under dense and sparse densities. Arf6 activities were measured by the GST-GGA pulldown method. Amounts of Arf6 protein in total cell lysates (10 μg) are shown below by immunoblotting. Erk1/2 activities in total cell lysates (10 μg) were assessed by anti-phospho Erk1/2 and anti-Erk1/2 immunoblots, as indicated. (B) Distribution of E-cadherin and ZO-1 in cells cultured under dense and sparse densities. E-cadherin was labeled using the ECCD-2 antibody coupled with an Alexa 488-labeled anti-rat IgG antibody. ZO-1 was labeled using an anti-ZO-1 antibody coupled with an Alexa 555-labeled anti-rabbit IgG antibody. Focuses were adjusted across the center of the majority of cell bodies, for the observation of E-cadherin. Projection images were used for ZO-1. Confocal images of the z-axis (indicated by yellow lines) are also shown at the bottom. Green, E-cadherin; magenta, ZO-1. Bar, 20 μm. (C) Arf6 and Erk1/2 activities during depletion and readdition of calcium ions. Activities of Arf6 and Erk1/2 were assessed as described in A. In A–C, these assays were performed at least three times, and representative figures are shown.

2001), are suppressed in MDCK cells cultured under a dense density as compared with a sparse density, whereas Arf6 protein levels do not notably differ between these two cell densities (Figure 1A). Suppression of Arf6 activity has been implicated in inhibition of the internalization of E-cadherin from cell–cell contact areas, as well as stabilization of the cell–cell contacts (Palacios *et al.*, 2001, 2002). Consistently, E-cadherin seemed to be more densely accumulated at cell–cell contact areas in cells cultured under the dense density than cultured under the sparse density, and this accumulation was accompanied by substantial reduction of the amount of E-cadherin molecules in the cytoplasm and in the apical areas of the cell surface (Figure 1B). Moreover, observation from the z-axis revealed that E-cadherin is more clearly segregated from a tight junction protein, ZO-1, as well as from an apical marker protein, Ezrin, in the dense cells than in the sparse cells (Figure 1B and Supplemental Figure S1), indicating enhanced apical-to-basal polarization of the dense cells compared with the sparse cells.

To obtain clues as to how E-cadherin–based cell–cell adhesions are involved in the suppression of Arf6 activity, we used the calcium switch assay (Zantek *et al.*, 1999), in which calcium ions are first deprived from the culture medium by the addition of EGTA and then added again. We found that Arf6 is swiftly activated upon EGTA treatment and then gradually down-regulated after readdition of calcium (Figure 1C). Activities of Erk1/2 have been shown to be increased by perturbation of E-cadherin–mediated cell–cell contacts in intestinal epithelial cells (Laprise *et al.*, 2004). We confirmed that activities of Erk1/2, as assessed by their phosphorylation, are also increased upon EGTA treatment and then gradually decreased after readdition of calcium in these MDCK cells (Figure 1C; also see below). Likewise, activities of Erk1/2 were suppressed in MDCK cells cultured under a dense density compared with a sparse density (Figure 1A).

Ligand Activation of EphA2 Suppresses Arf6 Activity and Induces Cell Compaction and Polarization

Among the EphA receptors, MDCK cells were found to predominantly express EphA2 (Supplemental Figure S2). We found that tyrosine phosphorylation of EphA2 is dramatically increased in MDCK cells cultured under the dense density compared with the sparse density (Figure 2A). In human mammary epithelial MCF-10A cells, tyrosine phosphorylation of EphA2 has been shown to be dependent on calcium ions in the culture medium (Zantek *et al.*, 1999). Consistently, tyrosine phosphorylation of EphA2 in MDCK cells, which was induced by culturing cells under the dense density, was substantially diminished upon EGTA treatment and was gradually recovered after readdition of calcium (Figure 2B). MDCK cells also express ephrinA1, and, to a lesser extent, ephrinA4 (Supplemental Figure S2), and the above-described enhanced activation of EphA2 under the dense cell density is likely to be due to paracrine stimulation of EphA2 by its ligands upon cell–cell contacting, which might occur more efficiently at the dense cell density than at the sparse cell density. In contrast, ephrins themselves are also known to transduce intracellular signals, upon binding to Eph receptors (Pasquale, 2005). We found that stimulation of MDCK cells, cultured under the sparse density, with ephrinA1 fused to the Fc portion of human immunoglobulin G (ephrinA1-Fc) down-regulates Arf6 activity, whereas a control Fc fragment or EphA2-Fc did not (Figure 2C). Dense tyrosine phosphorylation of EphA2 upon ephrinA1-Fc stimulation was confirmed under the same condition (data not shown). This ephrinA1-Fc stimulation of MDCK cells also induced cell compaction, which was accompanied by the enhanced accumulation of E-cadherin to cell–cell contact areas (Figure 2, D and E, Supplemental Figure S3 and Supplemental Video S1). Observation from the z-axis revealed that E-cadherin is more clearly segregated from ZO-1 and Ezrin in ephrinA1-Fc–treated cells than in control Fc-treated cells, indicating that these ephrinA1–Fc-treated cells were more polarized in the apical-to-basal direction, as seen with cells cultured under the dense density (Figure 2D and Supplemental Figure S1). Therefore, ephrinA1-stimulated MDCK cells resemble those cells cultured under the dense density, in their EphA2 phosphorylation, Arf6 activities, morphology and apical-to-basal polarization. We also found that treatment of MDCK cells with an anti-E-cadherin antibody, DECMA-1, which blocks E-cadherin function (Vestweber and Kemler, 1985), inhibits ephrinA1–Fc-mediated cell compaction (Figure 2F), suggesting the involvement of homophilic E-cadherin adhesion in this event.

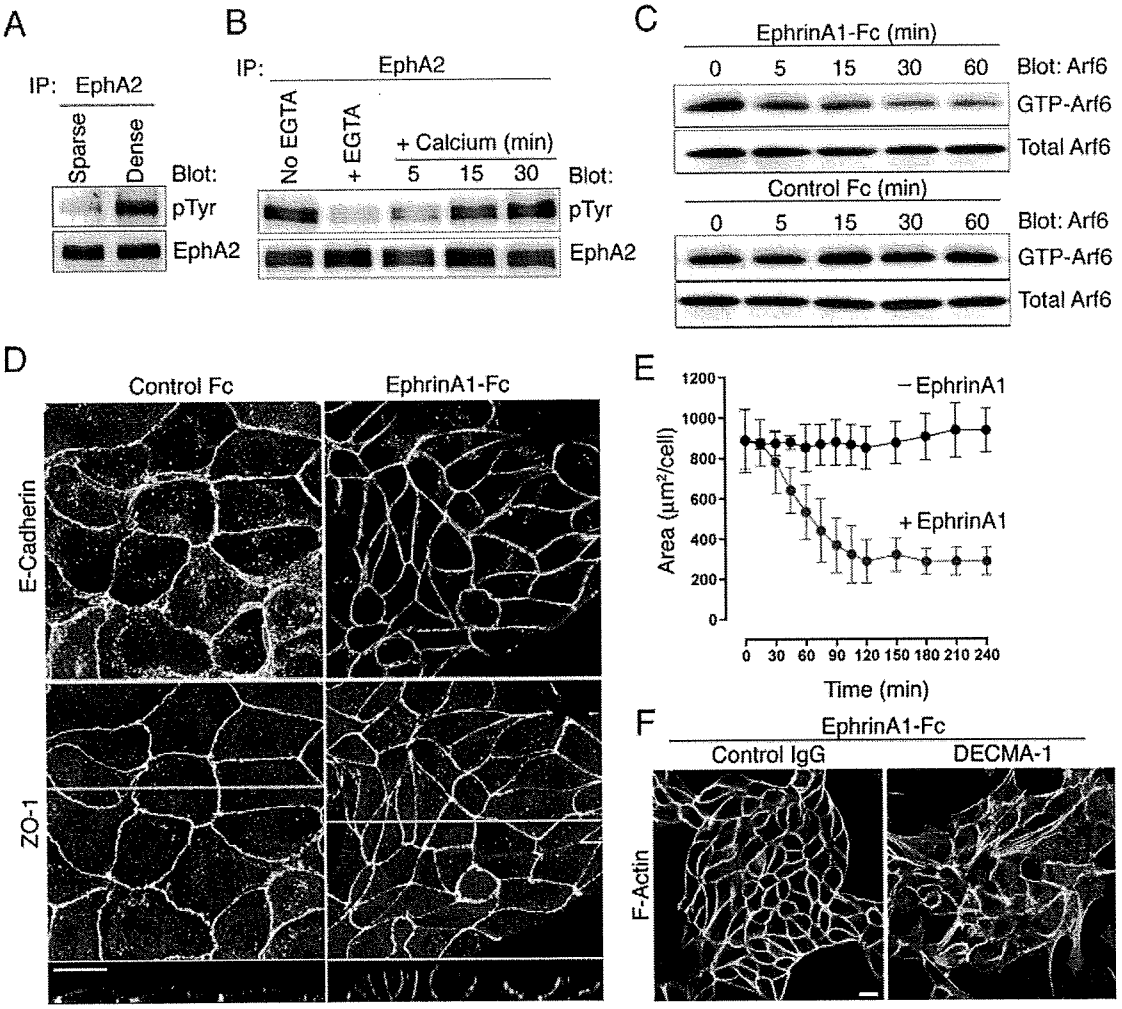

Figure 2. EphrinA1 stimulation causes Arf6 suppression, cell compaction, and apical-basal polarization in MDCK cells. (A and B) Tyrosine phosphorylation of EphA2 in cells cultured under dense and sparse densities (A) or during depletion and readdition of calcium ions (B) was assessed by immunoblotting as indicated. (C) Arf6 activities in cells cultured under the sparse density and treated with ephrinA1-Fc or control Fc for the indicated times. (D) E-Cadherin and ZO-1 distribution, as well as cell morphology, in cells treated with ephrinA1-Fc or control Fc for 3 h. Confocal images of the z-axis, indicated by yellow lines, are shown at the bottom. E-Cadherin and ZO-1 were visualized as shown in Figure 1B. (E) Time course of cell compaction upon ephrinA1 treatment. Cells expressing E-cadherin-Venus and cultured under the sparse density were subjected to time-lapse imaging in the presence or absence of ephrinA1-Fc, and their surface areas, as determined by E-cadherin-Venus–positive cell–cell junctions, were calculated. Error bars represent ± SEM from three independent experiments (n = 5 in each experiment). (F) Inhibition of ephrinA1-induced cell compaction by the DECMA-1 antibody. Cells cultured under the sparse density were pretreated with DECMA-1 (25 μg/ml) or control IgG for 30 min and then stimulated with ephrinA1-Fc for 3 h in the presence of DECMA-1 or IgG. Rhodamine-phalloidin staining of cells are shown. In A, B, and C, each assay was performed three times, and representative figures are shown. Total, 10 μg of total cell lysates. Bars 20 μm (D and F).

Dominant-Active Form of Arf6 Blocks EphrinA1-induced Cell Compaction

To assess whether ephrinA1–Fc-induced cell compaction is related to Arf6 activities, we next established MDCK cell lines stably expressing HA-tagged Arf6 and its mutants (Figure 3A). Expression of a guanosine triphosphate (GTP) hydrolysis-defective form of Arf6-HA, Arf6Q67L-HA, but not wild-type Arf6-HA, caused a spread out cell morphology, which was resistant to ephrinA1–Fc-mediated cell compaction (Figure 3, B and C). Such resistance to ephrinA1-Fc was not observed with a similar type of Arf1 mutant, Arf1Q71L-HA (Figure 3, B and C). In contrast, expression of a GTP binding-defective form of Arf6-HA, Arf6T27N-HA, induced cell compaction (Figure 3, A–C). However, expression of Arf6T27N-HA was very low compared with wild-type Arf6-HA and Arf6Q67L-HA (Figure 3A), and these cells expressing Arf6T27N-HA could respond to ephrinA1-Fc to become more compacted (Figure 3, B and C). These results are consistent with the notion that down-regulation of Arf6 activity plays an integral role in the pathway by which ligand-activated EphA2 induces cell compaction.

EphA2 Uses Git1 to Suppress Arf6 Activity

We then sought to clarify the mechanism by which ligand-activated EphA2 down-regulates Arf6 activity. EphA2 signaling pathways have already been extensively characterized (Pasquale, 2005). However, none of the known signaling pathways can adequately explain the suppression

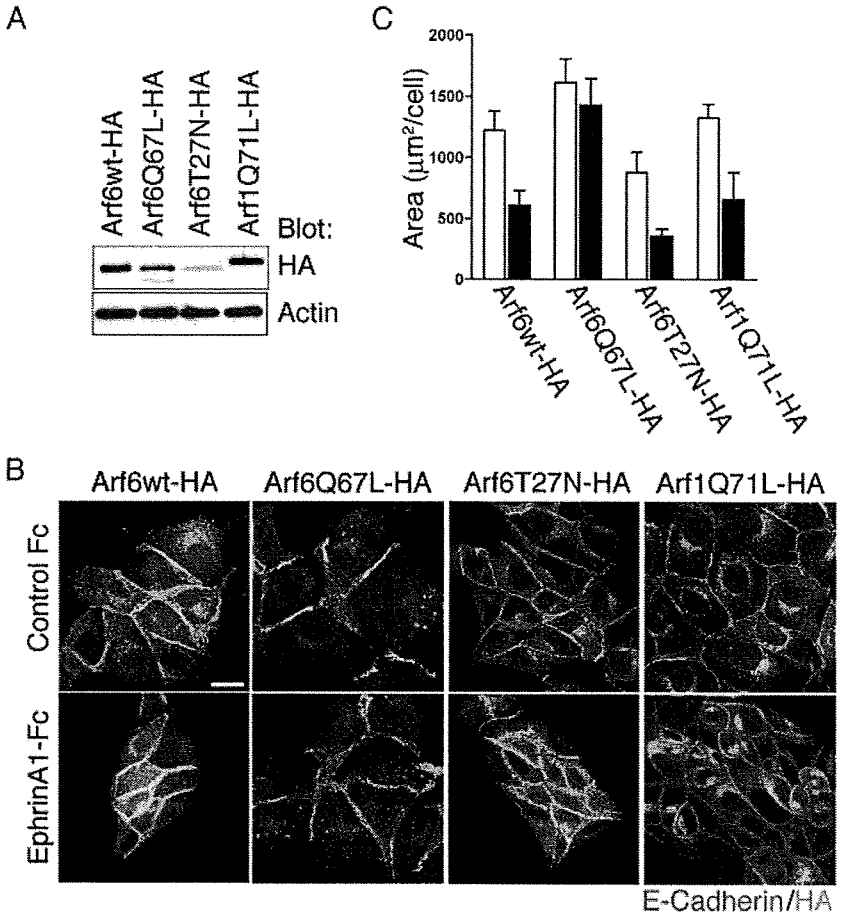

Figure 3. Arf6Q67L blocks ephrinA1-induced cell compaction in MDCK cells. (A) Expression of Arf6-HA, its mutants or Arf1Q71L-HA, as detected by anti-HA immunoblots. Anti-actin immunoblots are included as a control. (B and C) Morphology and E-cadherin distribution (B) and surface areas (C) of cells expressing HA-tagged Arf proteins and treated with ephrinA1-Fc or control Fc for 3 h. In B, E-cadherin was labeled by the ECCD-2 antibody coupled with an Alexa 555-labeled anti-rat IgG antibody (magenta) and HA-Arfs by an anti-HA antibody coupled with an Alexa 488-labeled anti-mouse IgG antibody (green). Bar, 20 μm. In C, open bars, control Fc; closed bars, ephrinA1-Fc. Error bars represent ± SEM from three independent experiments (n = 30 in each experiment).

of Arf6 by EphA2. We examined whether some GTPase activation proteins (GAPs) for Arf GTPases are linked to EphA2. Git1 exhibits efficient GAP activity against different Arf isoforms, including Arf6 (Premont *et al.*, 1998; Meyer *et al.*, 2006). We found that a significant amount of Git1 is coimmunoprecipitated with EphA2, when MDCK cells are stimulated by ephrinA1-Fc (Figure 4A). Conversely, an anti-Git1 antibody also coimmunoprecipitated significant amounts of EphA2, which was dependent on ephrinA1-Fc stimulation (Figure 4B). Git1 has a structurally conserved isoform, namely, Git2 (Hoefen and Berk, 2006). Git2 did not coprecipitate with EphA2 (Figure 4A). Consistent with these results, siRNA-mediated knockdown of Git1 substantially abolished ephrinA1–Fc-mediated suppression of Arf6 activity, as well as ephrinA1–Fc-mediated cell compaction and apical-to-basal polarization (Figure 4, C–F and Supplemental Figure S4). To confirm the specificity of the Git1 siRNA, we then established MDCK cells expressing a rescue construct of Git1-FLAG, in which the Git1 siRNA-target nucleotides were mutated (Figure 4C), and we confirmed that ephrinA1–Fc-mediated suppression of Arf6 activity, as well as ephrinA1–Fc-mediated cell compaction were still observed in these "rescued" cells, even when the cells were treated with the Git1 siRNA (Figure 4, D–F). These results suggest that EphA2, when ligand activated, uses Git1 to suppress Arf6 activity and that this engagement of Git1 is important for the EphA2-mediated modulation of cell–cell contacts.

Ligand-activated EphA2 is known to attenuate the activities of mitogen-activated protein kinases (Miao *et al.*, 2001). Moreover, the Arf6 GTPase cycle has been implicated in the activation of Erk kinases (Tague *et al.*, 2004). We however found that knockdown of Git1 does not affect ephrinA1–Fc-induced suppression of Erk1/2 activities (Figure 4D). Therefore, the EphA2–Git1 pathway down-regulating Arf6 activity is substantially independent of the EphA2 pathway down-regulating Erk1/2 activity in MDCK cells.

EphA2 Requires Nck1 to Associate with Git1

Git1 does not seem to have protein interaction modules that can directly bind to ligand activated EphA2. In contrast, Git1 has been shown to bind to several adaptor proteins, such as Nck (Frese *et al.*, 2006). Among the Nck isoforms, MDCK cells predominantly express Nck1 (Supplemental Figure S1). We found that Nck1 is readily coprecipitated with Git1 in MDCK cells even without ephrinA1-Fc stimulation (Figure 5A). In contrast, Nck1 coprecipitated with EphA2 only after ephrinA1-Fc stimulation of these cells (Figure 5A). Coprecipitation of Git1 with EphA2 was abolished upon siRNA-mediated knockdown of Nck1 (Figure 5, B and C). Similar to the Git1 knockdown, knockdown of Nck1 also abolished ephrinA1-Fc-mediated suppression of Arf6 activity (Figure 5D), as well as ephrinA1–Fc-mediated cell compaction and apical-to-basal polarization (Figure 5, E and F, and Supplemental Figure S4). Therefore, Nck1 seems to link Git1 with ligand-activated EphA2.

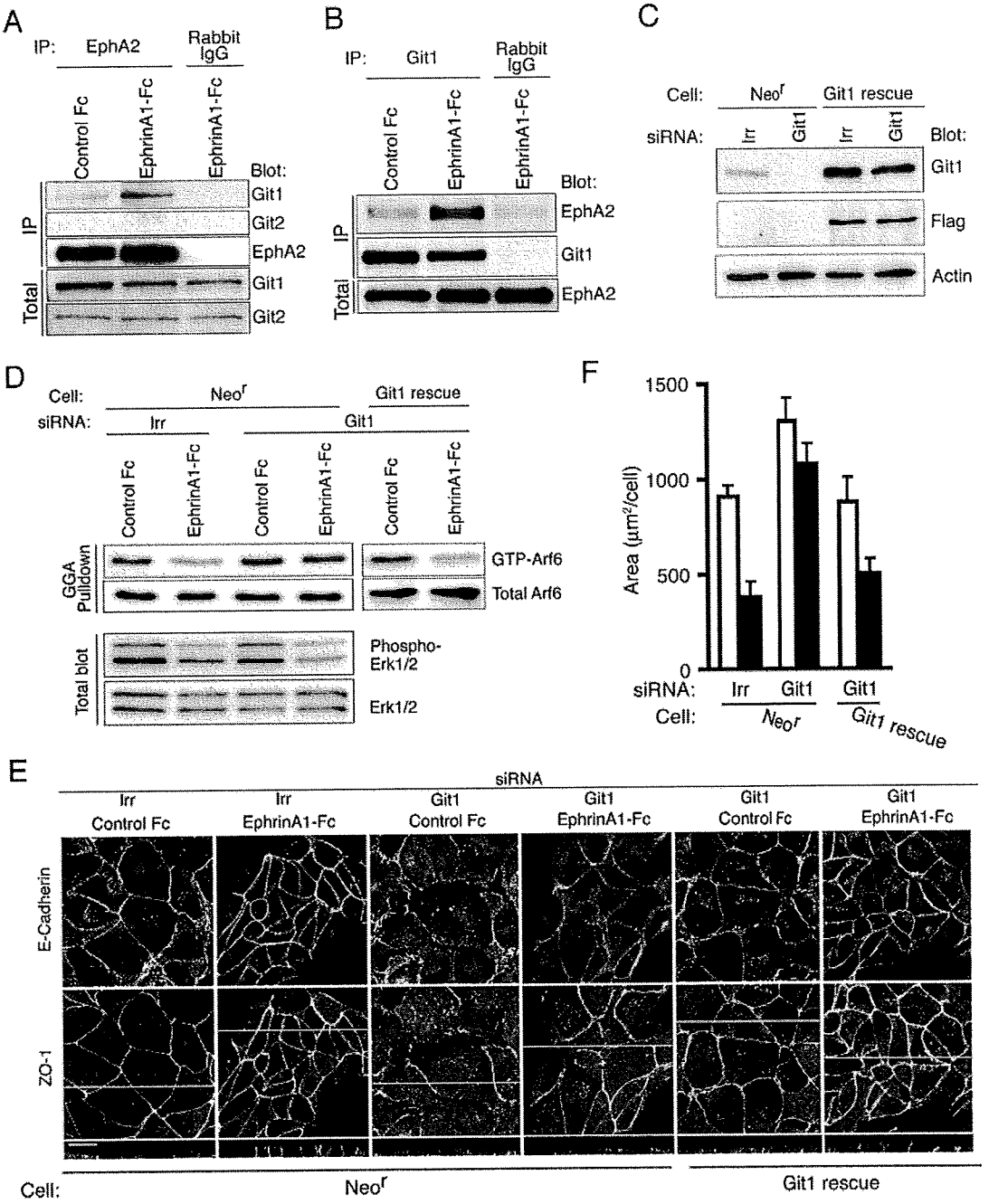

Figure 4. EphA2 requires Git1 for Arf6 suppression and cell compaction in MDCK cells. (A and B) Coprecipitation of Git1 with EphA2 upon ephrinA1-Fc stimulation. Cells cultured under the sparse density were stimulated with ephrinA1-Fc or control Fc for 30 min, and their EphA2 (A) or Git1 (B) was immunoprecipitated and analyzed for the coprecipitation of Git1 (A) and EphA2 (B) by immunoblotting, as indicated. Controls include nonspecific IgGs (rabbit IgG) and an anti-Git2 antibody, as indicated. (C–F) Requirement of Git1 for Arf6 suppression (D), and cell compaction (E and F), induced by ephrinA1-Fc. Cells stably transfected with pcDNA3 (Neo^r) or the FLAG-tagged Git1 rescue plasmid (Git1 rescue) were treated with Git1 siRNA or an irrelevant siRNA (Irr) and cultured under the sparse density. In D, cells were treated with ephrinA1-Fc or control Fc for 30 min. In E and F, cells were treated with ephrinA1-Fc or control Fc for 3 h. Endogenous Git1 and rescue Git1 expression (C) and cell surface areas (F) are also shown. In D, Erk1/2 activities in total cell lysates (10 μg) were assessed by anti-phospho-Erk1/2 and anti-Erk1/2 immunoblots, as indicated. In E, E-cadherin and ZO-1were labeled as described in Figure 1. Confocal images of the z-axis, indicated by yellow lines, are shown at the bottom. Bar, 20 μm. In F, open bars, control Fc; closed bars, ephrinA1-Fc. Other labels are the same as in Figures 1 and 2.

Precise Mechanisms of Formation of the EphA2–Nck1–Git1 Complex

The above-mentioned results indicate that the association of Nck1 and EphA2 occurs only after ephrinA1 stimulation, whereas that of Nck1 and Git1 occurs constitutively. We then investigated the precise mechanisms involved in the protein interactions of this EphA2–Nck1–Git1 complex. Because EphA2 makes a complex with Git1 upon ephrinA1-Fc

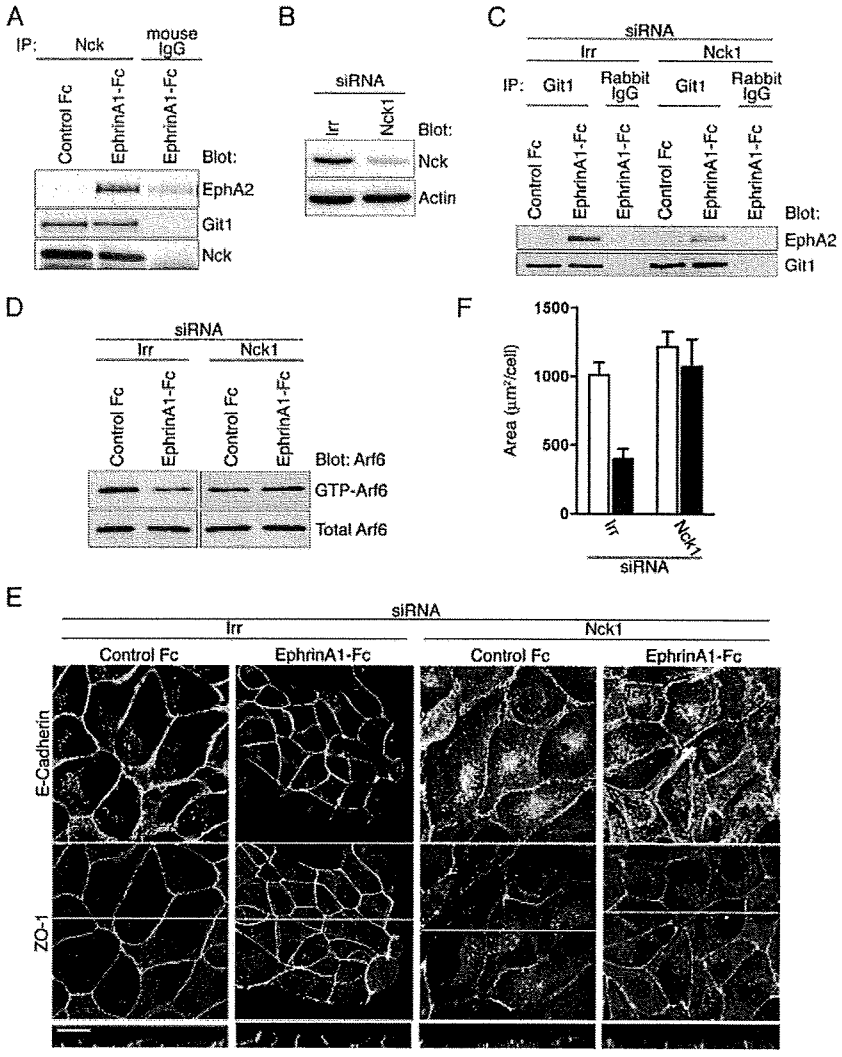

Figure 5. Nck links EphA2 with Git1 in MDCK cells. (A) Complex formation of Nck with EphA2 and Git1. Cells cultured under the sparse density were stimulated with EphrinA1-Fc or control Fc for 30 min, immunoprecipitated with an anti-Nck antibody and analyzed for coprecipitation of EphA2 and Git1 by immunoblotting, as indicated. Nonspecific IgGs (mouse IgG) were included as a control. (B–F) Cells were treated with an Nck1 siRNA or an irrelevant siRNA (Irr) and cultured under the sparse density. Requirement for Nck1 in EphA2-Git1 association (C), Arf6 suppression (D), E-cadherin and ZO-1 localization (E), and cell compaction (F), induced by ephrinA1-Fc, are shown. In C and D, cells were treated with ephrinA1-Fc or control Fc for 30 min. In E and F, cells were treated with ephrinA1-Fc or control Fc for 3 h. Nck1 expression in total cell lysates (10 μg) is also shown (B). In C, nonspecific IgGs (Rabbit IgG) are included as a control. In E, confocal images of the z-axis, indicated by yellow lines, are shown at the bottom. Bar, 20 μm. In F, open bars, control Fc; closed bars, ephrinA1-Fc. Other labels are the same as in Figures 1 and 2.

stimulation, we first examined the possible involvement of ligand-induced tyrosine phosphorylation of EphA2 in this complex formation. Phosphorylation of highly conserved tyrosine residues on the juxtamembrane region of Eph receptors, which correspond to Tyr588 and Tyr594 of EphA2, has been shown to be the major Nck binding sites (Kullander and Klein, 2002). We expressed Git1-FLAG in HEK293T cells together with HA-tagged EphA2 (EphA2-HA) or its tyrosine nonphosphorylation mutants Y588F and Y594F, in which Tyr588 and Tyr594 are mutated into phenylalanine, respectively (Figure 6A). HEK293T cells express Nck endogenously (Figure 6B). Moreover, EphA2 overexpressed in HEK293T cells was notably tyrosine-phosphorylated even without exogenous stimulation by ephrinA1-Fc (data not shown), similar to those observed with other Eph receptors overexpressed in HEK293 cells (Becker *et al.*, 2000). We found that mutation of Tyr594, but not Tyr588, substantially abolishes coprecipitation of EphA2-HA with Git1-FLAG (Figure 6B). We then examined whether phosphorylation of Tyr594 is necessary for the association of EphA2 with Nck1. Nck1 has one Src homology 2 (SH2) domain, a domain known to bind to phosphotyrosines. We found that a GST fusion form of the SH2 domain of Nck1 (GST-Nck1 SH2) binds to wild-type EphA2-HA and its Y588F mutant (EphA2 Y588F-HA) but not the Y594F mutant (EphA2 Y594F-HA) (Figure 6C).

We next investigated which portion(s) of Git1 is necessary for its complex formation with EphA2. It has been reported that Tyr392 of Git1 can be phosphorylated and that this phosphorylation enables its binding to the SH2 domain of Nck (Frese *et al.*, 2006). We however found that mutation of Tyr392 into phenylalanine (Git1Y392F-FLAG) does not affect its complex formation with EphA2-HA (Figure 6D). In contrast, we showed above that EphA2 does not associate with Git2 (Figure 6D). The synaptic localizing domain, present in Git1, is not well conserved in Git2 (Supplemental Figure S5). We found that the synaptic localizing domain-deletion mutant of Git1 (Git1ΔSLD-FLAG) no longer associates with EphA2-HA (Figure 6D). Consistently, the synaptic localizing domain of Git1 alone (Git1 SLD-FLAG) was able to associate with EphA2-HA (Figure 6D). The synaptic localizing domain of Git1 contains several repeats of proline-rich sequences at its C terminus, which apparently conform to Src homology 3 (SH3) binding motifs. Nck1 contains three tandem repeats of SH3 domains. Deletion of these proline-rich regions from the synaptic localizing domain of Git1 (Git1 SLDΔC-FLAG) abolished its complex formation with

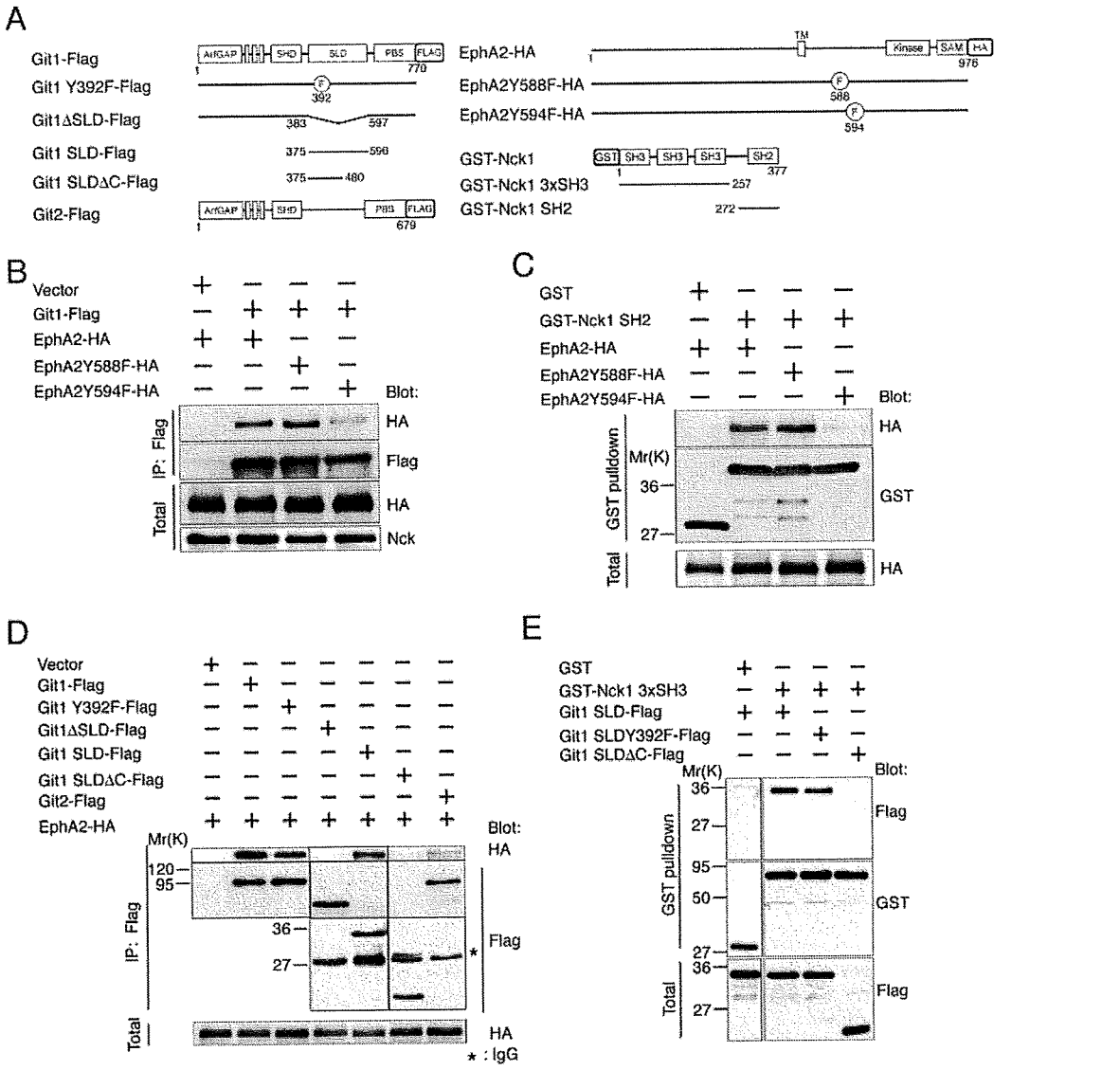

Figure 6. Mechanism of EphA2–Nck1–Git1 complex formation. (A) Schematic representations of EphA2, Nck1, Git1, and their mutants. (B) Requirement for Tyr594 of EphA2 in EphA2-Git1 complex formation. Git1-FLAG was coexpressed with EphA2-HA or its YF mutants in HEK293T cells, as indicated, and immunoprecipitated with an anti-FLAG antibody to analyze its association with EphA2 mutants. (C) Binding of EphA2 to the Nck1 SH2 domain. GST-Nck1 SH2 was coexpressed with EphA2-HA or its YF mutants in HEK293T cells, as indicated, and subjected to GST pulldown to analyze its association with EphA2 mutants. (D) Requirement of the synaptic localizing domain of Git1 in EphA2-Git1 complex formation. Git1-FLAG or its mutants were coexpressed with EphA2-HA in HEK293T cells, as indicated, and immunoprecipitated with an anti-FLAG antibody to analyze their association with EphA2. Git2-FLAG is also included as a control. (E) Binding of the Git1 synaptic localizing domain to the Nck1 SH3 domains. GST-Nck1 3xSH3 (three tandem SH3 domains of Nck1) was coexpressed with Git1 SLD-FLAG or its mutants in HEK293T cells, as indicated, and subjected to GST pulldown to analyze its association with the Git1 synaptic localizing domain and its mutants. In B–E, total, 10 μg of total cell lysates. GST or empty vector are also included as controls.

EphA2-HA (Figure 6D). We also confirmed that the SH3 domains of Nck1, fused to GST (GST-Nck1 3xSH3), bind to Git1 SLD-FLAG but not Git1 SLDΔC-FLAG (Figure 6E). Together, it is most likely that in the EphA2–Nck1–Git1 complex, the phosphorylated Tyr594 of EphA2 binds to the SH2 domain of Nck1, and the SH3 domains of Nck1 bind to the synaptic localizing domain of Git1. Our results also indicate that Tyr392 of Git1 is dispensable for its association with EphA2. Tyr392 is conserved in Git2, whereas the synaptic localizing domain is not. Lack of the synaptic localizing domain in Git2 may explain why Git2 is not directly engaged by EphA2.

Subcellular Distribution of Git1 and EphA2 in MDCK Cells

We finally examined the possible colocalization of Git1, and also its mutants, with EphA2. Because immunostaining of endogenous Git1 in MDCK cells was very weak, we stably expressed Git1-FLAG and its mutants in MDCK cells and visualized them by use of an anti-FLAG antibody (Figure 7A). EphA2 is known to localize to cell–cell contact areas (Zantek *et al.*, 1999). We found that although only a small amount of Git1-FLAG is localized to cell–cell contact areas when cells are cultured under the sparse density, a significant fraction is swiftly recruited to cell–cell contact areas